Decomposition of FDG-PET Based Differential Uptake Volume Histograms in Rectal Cancer Patients

James Schneider

Medical Physics Unit

McGill University, Montreal

August 2016

A thesis submitted to the Faculty of Graduate Studies and Research in partial fulfillment of the requirements for the degree of

MASTER OF SCIENCE

In Medical Physics

Table of Contents

Abstract

The use and analysis of FDG-PET data may lead to the ability to predict the response of patients to radiotherapy. This work describes the process of using functional data to define underlying biological sub-volumes within a tumour and exploring predictive properties that they may have. A cohort of 15 histopathologically determined rectal adenocarcinoma patients were collected for this study; all staged as T3N0 prior to preoperative endorectal brachytherapy treatments. At the time of surgery, 8 of the patients' disease had no significant response to radiation while the other 7 had no visible tumour remaining (complete response). Due to difficulty in contouring regions of purely healthy rectal tissue, a further investigation of background definition was performed. This resulted in the sampling of healthy muscle tissue for all PET scan slices containing tumour, and a set of slice-unique background values was determined for each patient. The PET data was then converted to signal-to-background ratio (SBR) images, and SBR values were extracted from regions of interest covering the extent of the disease. After creating a differential uptake volume histogram by binning these values, decomposition was performed using multiple analytical functions. For the cohort studied, the best decomposition was determined to be with six Gaussian functions, as verified by chi-square analysis. Furthermore, a comparison of the relative abundances of the four most glycolytic sub-volumes between the patients that responded well and poorly to radiation led to statistically significant differences. This suggests that with extensive pre-clinical studies with larger patient populations, as well as continued work and exploration into the definition of a trustworthy background, it may be possible to predict the response to radiotherapy with the process outlined herein.

Résumé

L'utilisation et l'analyse des données FDG-TEP pourrait permettre la capacité de prédire la réponse des patients à la radiothérapie. Cet ouvrage définit le processus d'utiliser les données fonctionnelles pour décrire les sous-volumes biologiques sous-jacents au sein d'une tumeur, et explorer les propriétés prédictives qu'elles pourraient avoir. Une cohorte de 15 patients d'adénocarcinome rectal déterminés histopathologiquement ont étés collectés pour cette étude, tous au stage T3N0 avant curiethérapie. Au moment de la chirurgie, 8 des patients ne présentaient aucune réponse significative tandis que 7 des patients n'avaient pas de tumeur visible. Suite à la difficulté de contourné les régions de tissue rectal sain, une enquête plus approfondie des valeurs de fond. Le résultat était un échantillonnage de tissu musculaire sain pour toutes les images TEP contenant tumeur et un ensemble de valeurs de fond spécifique à l'image ont été déterminées pour chaque patient. Les données de TEP étaient converties en images de rapport signal sur bruit (RSB), et les valeurs RSB extraient à partir des régions d'intérêt portant sur l'étendue de la maladie. Après avoir créé un histogramme différentiel d'absorption par le binning de ces valeurs, la décomposition a été performé en utilisant plusieurs fonctions analytiques. Pour la cohorte étudiée, la meilleure décomposition trouvée était celle avec six fonctions gaussiennes, et ceci a été vérifié par analyse chi carré. En outre, une comparaison des abondances relatives de ces volumes entre les patients qui ont répondu bien et pauvrement aux rayonnements a conduit à des différences statistiquement signifiant. Cela suggère qu'avec des études précliniques approfondies ayant une large population de patients, ainsi que le continument de poursuite et d'exploration de la définition de fond, il serait possible de prédire la réponse de radiothérapie.

Acknowledgements

First and foremost, I would like to thank my supervisor, Slobodan Devic, for his continued tutelage and assistance. No matter the time of day or day of the week, he was available to discuss and analyse any idea or problem that came up over the course of this project. To Jan Seuntjens and all the other professors in the Medical Physics program, thank you for running and organizing such a thorough and fascinating program and managing so well despite the numerous clinical and administrative responsibilities you also balance. To Te Vuong, Nada Tomic, Marc Hickeson, Robert Lisbona, and Francois DeBlois, thank you for your assistance in this project, and all the discussions regarding the past and future avenues of study. To Hani Hassoun and Rima Tulbah, thank you for taking time out of your schedule to acquire all the various patient data used throughout the project. For my fellow colleagues in the Medical Physics program, all the discussions, presentations, and journal clubs were invaluable in continuing to promote inquisitive and novel approaches to my work, as well as for keeping me updated on the many going-ons in our field apart from my main focuses. To my parents, family, and to my wonderful partner Margaret Gordon – thank you all so much for your kind words and patience, for your constant support throughout the efforts spent in order to make this degree a reality.

List of Tables

List of Figures

Chapter 1: Introduction

1.1: The Basics of PET Imaging

The 1895 discovery of the x-ray by Wilhelm Röntgen birthed the study of radiation, followed shortly by the 1896 discovery of natural radioactivity by Henri Becquerel. These discoveries and the many more that have followed them have significantly improved human life in many fields, not least of all medicine. With the advent of man-made radioisotopes in the 1930s, the development of radiopharmaceuticals began.[1] The word radiopharmaceutical comes from its two constituent parts – pharmaceutical from the fact that these compounds are administered and taken up by the body according to some pharmacological action, and radio, as attached to the pharmaceutical is a radionuclide which is capable of emitting observable radiation.[2] The advent of radiopharmaceuticals led to many various imaging modalities, including both SPECT and PET. The development of commercially available joint PET/CT scanners in 2001 has led to an explosion of growth in the availability of PET scans[3] and, as such, continued effort is deserved in determining novel or improved methods to incorporate this information that is now being collected.

The positron is the elementary particle which is fundamental to Positron Emission Tomography (PET) imaging. Positrons are the antiparticle of the electron, having the same mass and spin as electrons, while having a charge of equal magnitude with opposite sign. While positrons can be generated via multiple methods, the process of relevance in PET imaging is positron emission decay.[4] In this process, a proton in the nucleus of a radionuclide converts into a neutron (while emitting both a positron and an electron neutrino to carry away excess energy as kinetic energy). Figure 1 shows an emission event taking place as well as subsequent events. Once a positron is emitted, it gives off its kinetic energy via collisions with surrounding

particles. As the positron comes to rest, it interacts with an electron, binding together to form an extremely short-lived exotic particle known as a positronium, with an expected lifetime of roughly 10^{-10} seconds.[2] Particle and antiparticle then undergo an annihilation reaction, converting the masses of both particles into energy. The energy equivalent of each particle is 511 keV and, if they were perfectly at rest, the annihilation reaction would result in two 511 keV photons emitted 180° apart from each other.

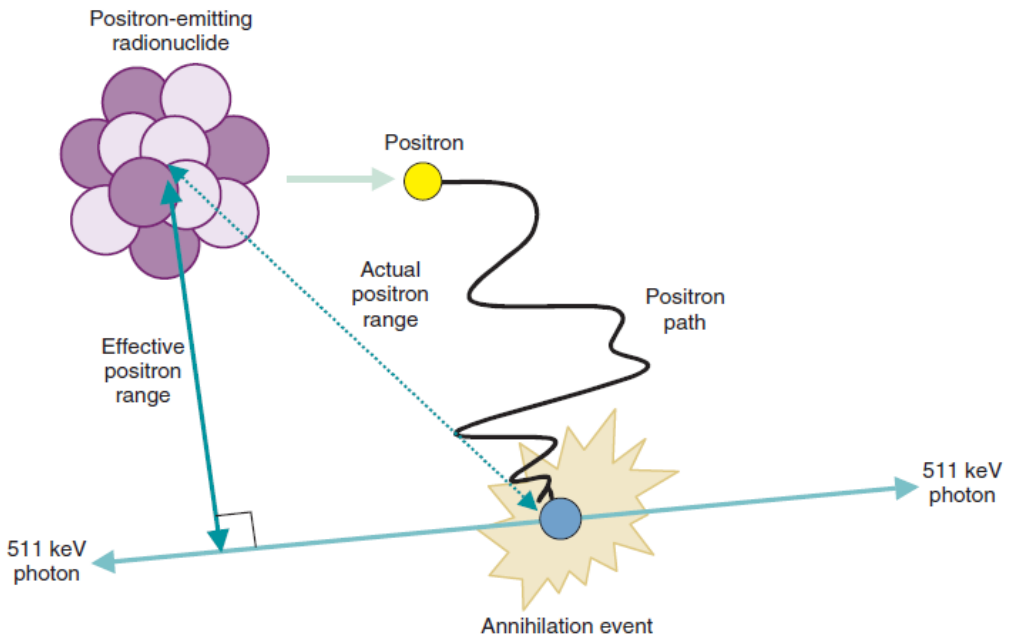

Figure 1: The process of positron emission and annihilation. Image adapted from Cherry, Sorenson, & Phelps[2]

A PET scan is performed by first injecting a radiopharmaceutical containing a positron emitting isotope intravenously into a patient.[2] After sufficient time is allowed for the radiopharmaceutical to circulate through the patient's body, the scan can begin. The crux of PET imaging lies in the capture of annihilation photons emitted from within a patient. In order to accomplish this, a PET scanner consists of multiple rings of detectors, typically four. Each ring is

made up of multiple block detectors which are scintillator crystals that have themselves been cut in order to create smaller crystal detectors. Each block detector is coupled to four photo-multiplier tubes (PMTs). Whenever a 511 keV photon is absorbed by a scintillator crystal, the crystal emits a pulse of light which is then amplified by the PMT, digitized, and analyzed.

Coincidence detection is an extremely important concept in the acquisition of PET images. Due to the underlying physics behind the annihilation process, it is possible to discard the signal from any photons captured without a corresponding 511 keV photon being captured at a detector nearly 180° away within a period of time known as the coincidence timing window.[2] This window typically corresponds to 6-12 ns, which can be compared with PET scanners' ability to time stamp acquired photons with a 1-2 ns accuracy. It also takes less than 2 ns for a photon to cross the diameter of the bore. Once two signals are found to lie within the coincidence timing window, a line of response (LOR) is determined between the two detectors, as many can be seen in Figure 2. The signals are summed and the energy acquired is checked against that expected. If the event meets the requirements, a memory location in a sinogram corresponding to the angle and position of the LOR detected is incremented.

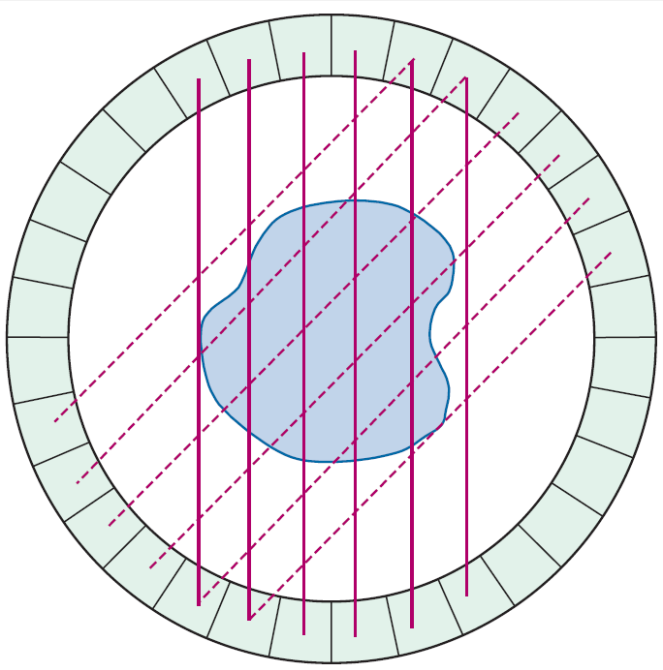

Figure 2: Schematic diagram of a PET scanner's array of detectors. Many lines of response (LORs) are shown connecting detectors opposite to each other. Image adapted from Cherry, Sorenson, & Phelps [2]

Once all the data are collected over the course of a scan, software is utilized to reconstruct images from the set of coincidental events. The number of counts occurring in each voxel corresponds to the spatial distribution of the radioisotope throughout the body, and thus the radiopharmaceutical. As the concentration and distribution of radiopharmaceutical are dependent on the physiological processes of the body, a colour or grey-scale image of the activity within the body is created.[2] The most common radiopharmaceutical used is FDG, discussed in depth in Section 1.2, which enables the mapping of glucose metabolism in the body.[3] The images created are thus innately quantitative, allowing the determination of spatial radiopharmaceutical concentrations.

The spatial resolution of a PET image is roughly four times worse than that of an MRI or CT image of the equivalent object.[2] There are multiple sources of this lower effective resolution.

First is the intrinsic resolution of the detector, R_{det}, which corresponds to the size of the actual individual elements of a detector. R_{det} is equal to half the width of the individual sensor element for a scanner with discrete detectors. As the average detector element is ~4 mm, this error (full-width at half-maximum) is roughly 2 mm. Next is the effective positron range (R_{range}): after being emitted by the radioisotope, a positron will travel some distance before meeting and annihilating with an electron. The effective label denotes that the distance is measured as a straight line from the point of emission to the point of annihilation. The difference between actual and effective positron ranges is shown in Figure 1. For the most commonly used isotope in PET imaging, F^{18}, the root mean square R_{range} is equal to 0.2 mm^2. R_{range} can belong to a spectrum of possible values, and as such is reported probabilistically. Photon non-colinearity (R_{180}) is another detrimental effect. When annihilation occurs, there is typically some small residual momentum associated with the positron which gets converted into an angular distribution with a full-width at half-maximum of roughly 0.5°. With the use of trigonometry, this has been shown to result in an image blur of 0.0022*D, where D is the diameter of the PET scanner bore[2]. This diameter is typically 80 cm for a whole body scanner, resulting in a 2 mm blur. Finally, there is the Block Effect (R_{BE}). This is an effect that is not very well understood, related to the use of block detectors in almost every modern day PET scanner. One potential cause of this effect lies within the use of detecting crystal cut from a single scintillation crystal.[5] This is proposed to lead to a loss of positioning accuracy depending on the depth of photon interaction. Other studies[6] have since shown that while this is a contributing factor, the blurring observed and described as the block effect is not purely a result of the use of block detectors and thus further studies are needed to investigate the exact cause of this effect and potential

improvements to PET detector design. Currently it is suggested to keep 1-2 mm blurring in consideration due to this effect.[6]

To get an overall system resolution from all these discrete degrading effects, their contributions must be added in quadrature.[2] This is based on the assumption that each effect can be approximated as a Gaussian blur to the true image. Taking note of the Convolution theorem, it has been shown that the convolution of multiple Gaussians result in a mean and variance (standard deviation squared) equal to the sum of all the individual means and variances, respectively. From this property of variances, the system resolution or the full-width at half-maximum for a system containing multiple Gaussian blurs is determined by addition in quadrature – in the case of PET scans with the aforementioned effects on spatial resolution:

$$R_{sys} = \sqrt{(R_{det})^2 + (R_{range})^2 + (R_{180})^2 + (R_{BE})^2}$$

With the estimates of these values given above, this results in the positron range being negligible for FDG-PET imaging, and the spatial resolution being 3-4 mm, roughly four times worse than CT/MRI, as mentioned earlier.

1.2: FDG-PET Imaging

There are numerous radiopharmaceuticals available for PET imaging. These arise from the many various combinations of radionuclides and radiotracers possible. The radionuclides used for PET scans typically consist of positron emitting isotopes that have short half-lives (fluorine-18 at roughly 110 minutes, carbon-11 at roughly 20 minutes, oxygen-15 at roughly 2 minutes, etc.). These half-lives are required to be short enough to emit a sufficient quantity of radiation to create images, but this results in the requirement of isotope delivery from a medical

grade cyclotron offsite (as is the case with the fluorine-18 used in this study) or in the case of the shortest-lived isotopes, an onsite investment in isotope production.[7] Of all the available radiopharmaceuticals, the most adopted for clinical use is, by far, the glucose analog 2-Deoxy-2-[^{18}F]fluoroglucose, known as [^{18}F]FDG, ^{18}F-FDG or simply FDG. This is in part due to both the economics of radiopharmaceutical production as well as to its proven use in the detection and staging of cancer.

In order to understand why FDG imaging represents one of the most appropriate imaging modalities for primary and metastatic cancers, it must first be understood how glucose is used by healthy cells and how cancerous cells typically differ. Figure 3 illustrates the full metabolic pathway that a glucose molecule takes, for both normal and cancerous cells.[8] Starting with a single glucose molecule, glycolysis occurs in which the glucose is broken down into two pyruvate molecules (pyruvic acid), with a net gain of two adenosine tri-phosphate (ATP) molecules which are the cell's main energy storing molecules. In the absence of oxygen, the metabolic process ends here, and the pyruvate is converted into lactic acid by the lactic acid cycle. If there is enough oxygen, the metabolic pathway continues differently. The two pyruvate molecules are converted into two molecules of acetyl coenzyme A (acetyl-CoA), which feed into the Krebs cycle. The Krebs cycle converts these acetyl-CoA molecules into six NADH (nicotinamide adenine dinucleotide) and two FADH (flavin adenine dinucleotide) molecules (both are electron carriers) and two more ATP molecules. Finally, NADH and FADH donate their electrons to the electron transport chain, creating a proton gradient that allows the creation of up to 34 ATP molecules.[8]

Figure 3: The metabolic pathways of glucose metabolism in both normal and cancerous cells, with and without the presence of oxygen. Image adapted from Devic [9]

In total, the process of aerobic cellular respiration results in a theoretical net of 38 ATP molecules per glucose molecule consumed[10]. Inefficiencies in this process as well as the energy required to shuttle the various molecules around lowers this number slightly in practice. This is in contrast to the much more inefficient 2 ATP molecules resulting from anaerobic glycolysis. In a healthy cell, it has been shown that the presence of oxygen inhibits the lactic acid cycle by converting pyruvate into acetyl-CoA in what is known as the Pasteur Effect.[11] A unique hallmark of most cancerous cells is the continued conversion of glucose into lactic acid, regardless of the presence or absence of oxygen. This aerobic glycolysis is also known as the Warburg effect. [12] Warburg's initial hypothesis stated that cancer was caused by the impairment of mitochondrial metabolism. This causal relationship has been since disproven, however multiple studies have continued to observe the Warburg effect in cancerous cells.[10]

The reliance on glycolysis alone for energy is extremely inefficient, given that the amount of glucose consumed by a human is not infinite. Furthermore, the production of lactic acid and other metabolic products associated with the lactic acid cycle (for example, hydrogen ions) causes an increase in the acidity of the extracellular space, and this can potentially lead to increased cell toxicity. [13] Despite this, the majority of cancerous cell populations routinely convert to this inefficient and harmful phenotype. It has been suggested that this response of cancerous cells is an adaptive response to the cellular environment experienced in the process of tumour growth.[14] Studies have gone on to demonstrate that tumour cells with this increased glycolytic activity have an increased production rate of a glucose transport protein known as Glut-1, in order to assist in obtaining access to the increased number of required glucose molecules.[15] Furthermore, it was shown that FDG uptake correlated with the level of Glut-1 as determined by a histological sample.

The increased metabolism of glucose and the promotion of enzymes and proteins to enable this metabolism is one of the defining features of cancerous growth. The link established between these traits and the presence of PET tracers like FDG suggest that not only can FDG-PET be used as a diagnostic tool, but that it can potentially be used to define and determine underlying regions of tumour physiology –biological target volumes – based on the local levels of glycolytic activity.

1.3: Literature Review

Since the introduction of PET to the clinic, numerous studies have been performed to both improve and advance the performance of the PET/CT scanner. In addition to this, numerous efforts have gone towards determining the best way to include PET data into routine use. The goal of this review is to summarize and discuss some of the directions academic studies have taken to incorporate PET into the clinic as both a target delineation as well as prognostic tool, leading into our goal of defining biological target volumes (BTVs) and our investigation of their possible predictive potentials.

1.3.1: The Introduction of PET to the Clinic

For the majority of modern radiotherapy, treatment planning has revolved around the concept of several anatomical objects. As codified in ICRU Report No. 50, the starting point is the gross tumour volume (GTV), consisting of the visible and macroscopic extent of malignant growth.[16] The clinical target volume (CTV) includes the GTV and an extended margin for the microscopic extent of malignant disease that has been shown to lie past the visible tumour volume and require treatment, as well as any other regions involved such as lymph nodes. Finally, the planning target volume (PTV) is another extension of the geometric target, taking

into consideration practical aspects such as equipment (limitations in setup and positioning) or anatomical (breathing or heart motions) uncertainties.

Computed tomography (CT) is the modality most widely used to define these various volumes. This is due to CT's great spatial reproducibility and ability to determine electron densities of tissues. Poor soft tissue contrast, a problem inherent with CT, led to the introduction of magnetic resonance imaging (MRI) to treatment planning. With the development of these imaging modalities, the ability to define an anatomical object has been greatly enhanced. Despite these improvements, these images still take only anatomical structure into consideration as the accepted belief was that a uniform dose delivered to the PTV would be sufficient for tumour control. With the advent and proliferation of PET/CT scanners, functional information has become more accessible than ever.[17] Combined PET/CT scanners also allow for a much improved PET image reconstructed process. Previous PET scanner models required external transmission scans performed with a radioactive source to acquire attenuation correction maps. A CT acquisition instead provides an attenuation correction map by itself.[18] Due to this advantage, PET acquisition time has been halved compared to earlier models.

The fact that previous work[19] has demonstrated a non-uniform functional behaviour of tumours has led to the development of the concept of biological target volumes (BTVs) - creating outlines not solely based on anatomical structures, but on localized tumour metabolic activity.[20] There are many questions that can be asked of PET imaging: How can PET be used to assist CT-based radiotherapy treatment planning? Can PET itself lead to accurate BTV definition? And finally, can these BTVs, once defined, be used to assist in predicting radiotherapy treatment outcomes? The goal of this thesis is to attempt to address these questions.

1.3.2: PET Based Target Delineation in Radiotherapy

While having a convincingly distinct role in the staging process, PET/CT imaging is a relatively new modality for radiotherapy target delineation, and various guidelines have been proposed. The initial commonly used methods for tumour outlining employing PET were: (1) the Qualitative Visual Method (QVM),[21] (2) Gross Tumor Volume (GTV) = 2.5 standardized uptake value (SUV) units;[22] (3) Linear adaptive SUV threshold function method;[23] and (4) GTV = 40% of local maximum uptake value (GTV_PET_40).[24] The QVM was used extensively in early attempts to incorporate PET information into the radiation treatment planning process.[25-31] The QVM carries personal bias and depends on the window and level set on the PET image by the person performing the target outlining.

The SUV is a useful quantity for diagnostic radiology, where the nuclear medicine specialist has to make a binary decision on whether or not the subject has an abnormal uptake in a certain region of the body. However, the SUV as a quantitative expression of the functional activity was argued to be inadequate for radiation treatment planning.[24] Alternatively, for the purpose of target delineation Erdi et al.[24Error! Bookmark not defined.] recommended the use of the "signal to background (S/B) ratio" and argued that the difference between the S/B ratio and the SUV is that the S/B ratio reflects the background activity specific for each local normal tissue, rather than making an assumption that the activity is uniformly distributed over the whole body. Thus, in contrast to the SUV definition, calculation of the S/B ratio accounts for physiological differences in local normal tissue or organ density and metabolism amongst patients.

Following these attempts for target thresholding, numerous variations of the four approaches outlined above have been developed over the years, with the goal of integrating PET

into the radiotherapy treatment planning process. In the following section, I will provide an overview of some of the many methods currently or previously developed for these goals. The methods presented herein are primarily used for outlining the GTV using PET and we wish to show that this may perhaps not be the most appropriate use of PET in treatment planning, prior to fully introducing the concept of a biological target volume (BTV) investigated in this work.

1.3.2.1: Percentage of maximum uptake threshold methods

Based on phantom measurement data, Erdi et al.[24] proposed using a fixed percentage (40%) of the maximum uptake signal-to-background ratio value as the threshold for defining the GTV. This was done despite the fact that the same paper pointed out that a threshold value should not be fixed because the best threshold value was determined to be target size dependent. Afterwards, the fixed threshold approach was adopted in many clinical studies.[32-36] This target size dependence effect has been subsequently investigated by many researchers and found to be real.[37-40]

Brambilla et al.[40] reported on the role of target-to-background ratio and target size for threshold segmentation for PET target volume delineation in radiation treatment planning. They adopted a multivariable approach to study the dependence of the threshold used to define the boundaries of FDG positive tissue on: the emission scan duration, the activity at the start of acquisition for different target sizes, and the target-to-background (T/B) ratios. An anthropomorphic model was used to study this dependence in conditions resembling the ones that can be encountered in clinical studies. An annular ring of water bags 3 cm thick was fitted over an International Electro-technical Commission (IEC) phantom in order to obtain counting rates similar to those found in average patients. They found that both the target size and the T/B

ratio play a major role in explaining the variance of the percentage threshold throughout the whole range of target sizes and T/B ratios examined.

1.3.2.2: Adaptive Thresholding methods

In the previous sub-section, the issues with a fixed threshold were described, including that of target-size dependence on optimal threshold value. As such, numerous researchers decided to investigate thresholding methods that were capable of adapting to the desired target. Black et al.[23]**Error! Bookmark not defined.** proposed an advanced adaptive thresholding method for target delineation using PET images in which threshold value varied with the size of the target. However, this study employed SUV, which does not represent the quantity of choice for the radiation treatment planning segmentation as mentioned previously, for reasons of patient and machine-specificity among others.[24]**Error! Bookmark not defined.**

Moving away from SUV values, El-Bassiouni et al.[41] suggested that for head and neck cancers different threshold values of tumour maximum uptake ratios (THR), depending on the actual maximum uptake magnitude (S), should be used to outline a PET-based GTV that effectively mimics a CT-based GTV. They suggested using 20% of THR for S > 30 kBq/ml, and 40% of the THR for S ≤ 30 kBq/ml.

Schaefer et al.[42] reported on the feasibility of instead using a contrast-based algorithm for PET-based delineation of the GTV in primary lung cancer patients. The authors defined image contrast as: $C = (mSUV_{70} - BG) / BG$ where BG is the mean background SUV, and $mSUV_{70}$ represents the mean SUV of the region-of-interest (ROI) surrounded by a 70% isocontour that was used to represent the FDG accumulation of each differently-sized sphere within the phantom

used. The authors concluded that the threshold SUV value (TS) could be approximated by a linear relationship $TS = a \cdot mSUV70 + b \cdot BG$, and then used for the delineation of PET-based GTV in lung cancer patients.

Aristophanous et al.[43] reported on the Gaussian mixture model (GMM) based segmentation technique on selected PET tumour regions for NSCLC patients. A GMM relies on the idea that any distribution, in this case, a distribution of image intensities, can be expressed as a mixture of Gaussian densities representing different classes. According to their implementation, each class belongs to one of three regions in the image where they attempted to obtain the tumour volume: the background, the uncertainty, and the target. The authors demonstrated that GMM gave a better congruence between PET-based and CT-based GTVs when compared to the fixed 40% maximum uptake threshold method. This methodology was one of the initial inspirations (alongside Ling et al.[20]) for this work. However, they chose to utilize it for the purpose of redefining GTVs instead of searching for other underlying sub-volumes.

Li et al.[44] reported on a PET tumour delineation method based on adaptive region-growing and dual-front active contours. First, a region of interest is manually drawn by a radiation oncologist that encloses a tumour. The voxel having the highest intensity in the ROI is chosen as a seed point and an adaptive region growing algorithm successively appends to the seed point all neighboring voxels whose intensities (T) are larger or equal to the mean of the current region. Change in T from 100% to 0% signifies a sharp volume increase, indicating the transition from the tumour to the background. A preliminary tumour boundary is determined just before the sharp volume increase, which was found to be slightly outside of the known tumour in all tested phantoms. A novel active contouring model is then applied to refine the preliminary

boundary automatically. The authors tested the applicability of the method by comparing the PET-based volumes to the known phantom volumes, or the CT-based GTV on patient data.

1.3.2.3: Iterative Thresholding methods

Further attempts at PET-based GTV delineation have attempted to utilize iterative algorithms to improve the final result. The following list of thresholding methods is only a brief overview of an extensive variety of methods tested over the years with intentions to incorporate PET data in target definition for radiotherapy treatment planning.[45] A more comprehensive review on this topic was presented by Zaidi and El Naqa.[46]

Van Dalen et al.[47] proposed a novel iterative method for tumour delineation and volumetric quantification with FDG-PET using background-subtracted relative-threshold levels (RTL). The method is based on a convolution of the point-spread function and a sphere with a certain diameter. These spherical functions were used as a first-order approximation for the shape of a tumour. Phantom data have validated that the theoretically optimal RTL depends on the sphere size: RTL=40% (D=15–60 mm), and RTL>50% for small spheres (D<12 mm).

Drever et al.[48] proposed another iterative threshold segmentation method for PET target volume delineation. A phantom study employing spherical targets was used to determine local (slice specific) threshold levels which produced correct cross-sections based on the contrast between target and background. Functions were fit to this data and used to construct an iterative threshold segmentation algorithm. Iterative threshold segmentation was applied using both an axial and tri-axial approach to the spherical targets and also to two irregularly shaped volumes. Of these two approaches, the tri-axial method proved less susceptible to image noise and better at

dealing with partial volume effects at the interface between target and background. For comparative purposes, single thresholds of 28% and 40% were also applied to the spherical data sets. The tri-axial iterative method was found capable of delineating cross sections with areas greater than 250 mm^2 to within the maximum resolution possible (1-pixel width). Cross sections of less than 250 mm^2 in the area were resolved by the tri-axial method to within 2-pixel widths of their true physical extent.

1.3.2.4: Drawbacks

A drawback of these approaches that use PET data to define gross target volume is that they create a single PET-based target volume that replaces the traditional CT-based GTV. Ignoring the underlying tumour physiology in the course of radiotherapy treatment planning in the past has mainly been due to the lack of wide-spread functional imaging resources. In the very same way, current efforts to replace the anatomical information with the functional image data has had the same deficiency in excluding the two complementary sources of information on tumour anatomy and physiology. All current quantitative thresholding methods rely on phantom measurements that sample a spatial distribution of a uniformly distributed FDG within a closed and rigid volume. Such an approach more closely resembles the known anatomical CT-based method based on geometry rather than the real patient-specific physiological activity.

Nestle et al.[49]**Error! Bookmark not defined.** have shown on a group of 25 NSCLC patients that when actual patient data are used, there is no correlation between any of the thresholding methods and the CT-based target volumes which are still assumed to be the "gold" standard for radiotherapy treatment planning. Similar studies comparing different thresholding methods on NSCLC patients[50] and head and neck cancer patients[51],[52] have reached the same conclusion. To illustrate the magnitude of differences in PET-based GTV contours outlined using some of the

methods listed above, Figure 4 shows an example of various contours on the same PET image. While the thresholding methods illustrated are all based on theoretical or experimental considerations, this figure raises uncertainty about how one can determine which method provides an acceptable surrogate for a CT-based GTV. As will be discussed in detail in Section 1.4 below, the goal of this project was to attempt not to continue to redefine the GTV with the use of PET, but to instead explore the definition and use of biological target volumes based on the functional data within and to evaluate the potential use of these volumes in the clinic.

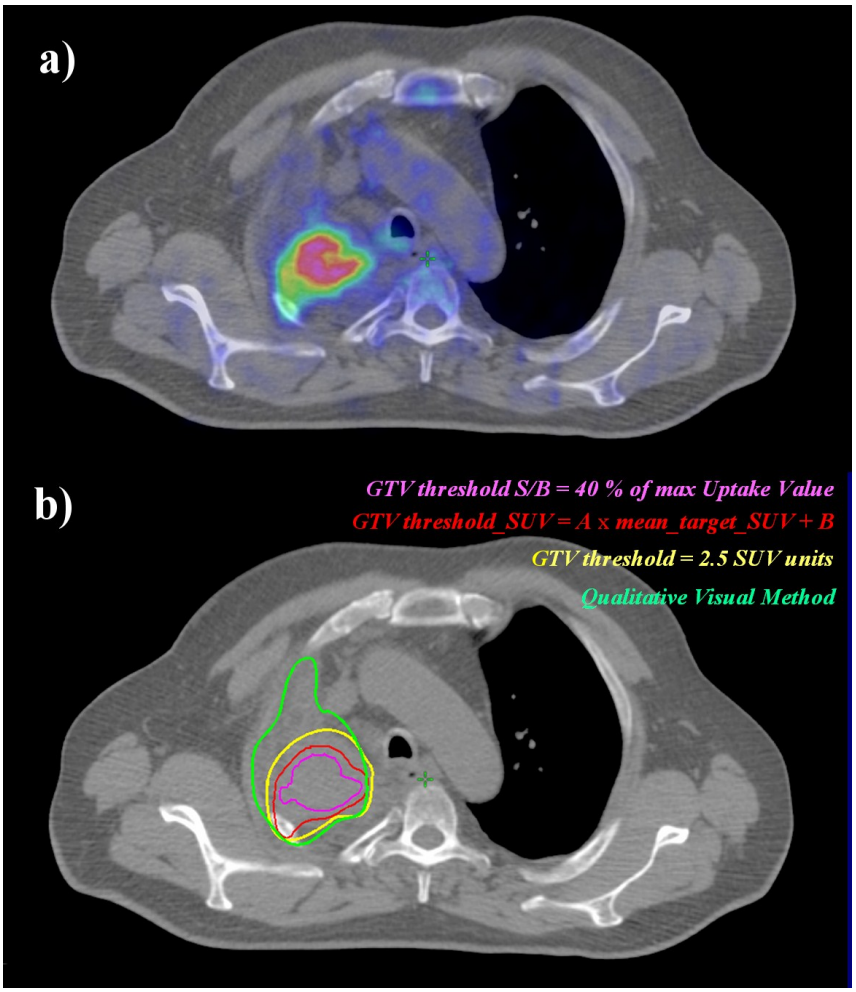

Figure 4: Various thresholding methods for GTV outlining on a PET Image: a) Co-registered PET/CT image of an NSCLC patient; b) Various contours following multiple guidelines (see Section 1.3.2) for GTV outlining on a PET image superimposed over the corresponding CT slice.

1.3.3: PET Based Treatment Evaluation

Many reports and papers have been published with the goal of determining the response of patients to either a portion of or the complete course of treatment, as well as predicting their long-term outcomes. In this section, we concentrate on published data related to rectal adenocarcinomas only.

One such study by Guillem et al.[53] found that for a cohort of 15 patients with locally advanced primary rectal cancer, FDG-PET scans performed before and after preoperative radio- and chemotherapy were able to potentially predict recurrence. This study utilized the changes in SUV_{max} at the time of a 42-month follow-up; the mean change in SUV_{max} was 69% and 37% for disease-free patients and those with recurrence respectively. This therefore presents a successful attempt at predicting the potential outcome of radiotherapy based upon the biological information contained within a PET scan. However, another more recent study by Ruby et al.[54] of 127 locally advanced rectal cancer patients found that no FDG-PET parameter studied [including average SUV, SUV_{max}, total lesion glycolysis (mean tumour SUV multiplied by tumour volume; TLG), and visual response] had a statistically relevant prognostic use when assessing rectal cancer response to chemoradiotherapy.

Hatt et al.[55] studied a cohort of 28 locally advanced rectal cancer patients who had scans acquired pre-treatment and at one- and two-weeks after preoperative chemoradiotherapy. This paper found that of all the pre-treatment parameters studied, only the average SUV value was correlated with response. Interestingly enough, a higher average SUV value for the tumour was predictive of better tumour response to therapy than lower average SUVs. In this study, no parameter comparison between baseline and one week after treatment was able to predict response, and the authors argue that this was caused by the difficulty in reproducing PET images

combined with the fact that allowing only one-week's passing did not allow for a robust parameter evolution. At the two weeks post-treatment scan, it was determined that TLG reduction was the best predictor of potential response, as well as average SUV to a lesser extent.

Moving beyond pure SUV values as the most studied prognostic parameter, Park et al. [56] found that the best results in predicted pathologically complete response was to normalize SUV_{max} to the average signal acquired within the liver (SLR) for a cohort of 88 locally advanced rectal cancer patients. The major finding was that a lower SLR calculated one week after chemoradiotherapy resulted in the best predictive capability for a complete response. The only predictive parameter acquired prior to treatment was tumour volume as calculated by a 2.0 SUV threshold. Other methods tried included the unnormalized SUV_{max}, normalization instead to the blood pool uptake, as well as tumour volumes as defined by various SUV thresholds.

In conclusion, numerous attempts have been made to predict response to radio(chemo)therapy for rectal cancer patients. Multiple parameters have been studied, both pre- and post-treatment to varying levels of success. However, the fact that SUV typically tends to be the by-far most studied variable is concerning, as discussed in Section 1.3.2, it is very patient- and machine-specific. In this work, we wish to attempt to define biological target volumes and to test their potential role as predictive values.

1.4: The Argument for Biological Target Volumes (BTVs) and Project Goals

Prior to the introduction and clinical acceptance of PET/CT scanners, anatomical data was the essential component in the treatment planning process.[57] One downside to the variety of approaches to PET-based treatment planning described in Section 1.3 is that the end-result is typically a PET-based replacement of the GTV, which is traditionally defined on CT. While obviously immensely useful for determining nodal involvement or metastases, when it comes to defining a GTV based on PET imaging, multiple studies come to the same conclusion: that the methodology boils down to using the best judgement of the radiation oncologist. [58]

The goal of this project is not to continue the attempts to redefine the anatomical GTV with PET data. We instead propose to explore and define the concept of biological target volumes based on the functional data of tumour physiology provided by FDG-based PET imaging as a complementary set of information. The concept of a Biological Target Volume originated in 2000 with the seminal paper by Ling et al.[20] The authors of this paper propose that in addition to the GTV, CTV, and PTV, a theoretical movement towards defining biological sub-regions of a tumour, potentially described as Biological Target Volumes (BTVs) as shown in Figure 5, should be undertaken.

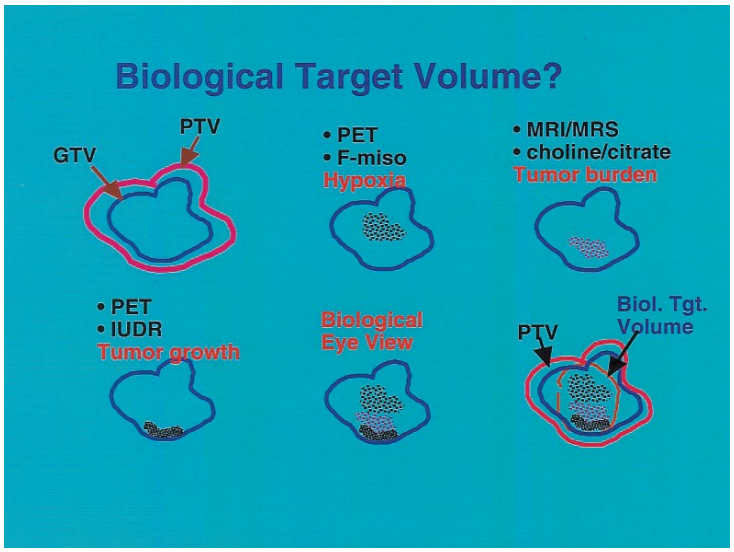

Figure 5: Creation of biological target volumes with functional information to complement existing anatomical information. Image adapted from Ling et al.[20]

The concept that tumours are not biologically homogenous has been observed well before PET/CT scanners had become widely adopted clinically. Figure 6 shows an extreme example of this for a large lung tumour. A line profile through the CT image on the left shows an essentially uniform level of anatomy. Meanwhile, a line profile through the PET image on the right shows its glycolytic activity; the tumour's physiology is varied, and glycolysis is concentrated primarily in the outer area. The idea of treating a tumour not as a uniform structure, and instead as a series of biologically different volumes is presented (in an admittedly oversimplified manner) in Figure 7's adaptation of Rene Magritte's famous piece of art – This is not a tumour!

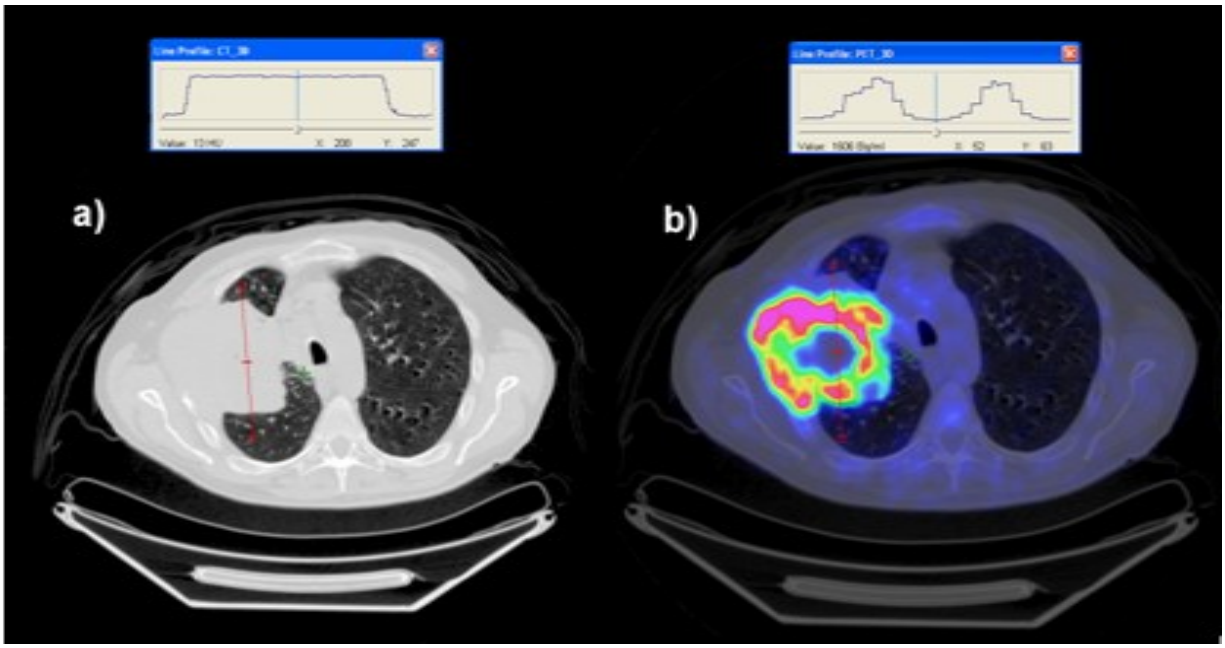

Figure 6: A comparison of CT (a) and PET (b) for a large lung tumour. Image adapted from Devic et al. [50]

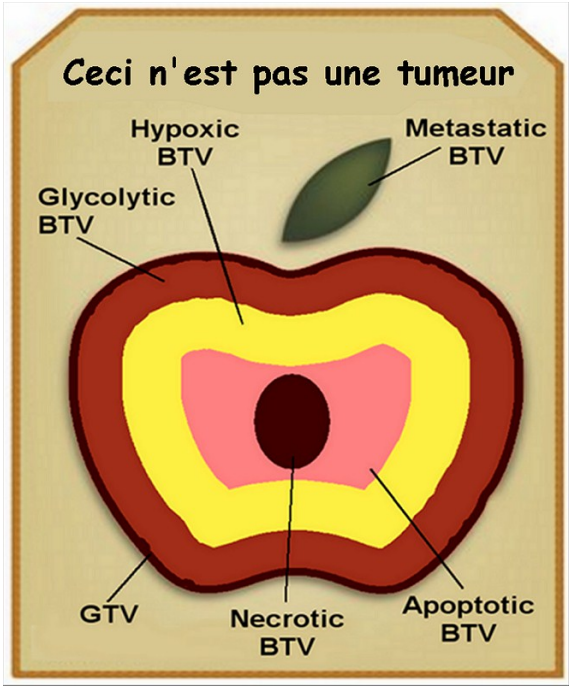

Figure 7: A lighthearted schematic of BTVs in the style of Rene Magritte (1928–29). Image adapted from Devic et al.[59]

One of the most important quantities when discussing the biology of a tumour is the oxygen diffusion distance. First calculated in 1955, it was determined that 145 μm was the rough radius from which a tumour could remain adequately supplied with oxygen.[60] A tumour in standard conditions tends to expand due to the rapid proliferation of the outermost layer of cells. As this occurs, the cells at the center of the tumour become more and more isolated from blood vessels and thus oxygen supply. Hence, once a tumour begins to grow past a certain size, a resultant inner region begins to experience cell death.[61] This can occur either via apoptosis – where cells undergo programmed death when placed in such a profoundly stressful situation, or via necrosis, in which the external factors become so extreme (typically associated with cancer malignancy) that the cells die in an unregulated manner.[62] Lying in between the region of oxygenated, proliferating cancer cells and the inner region of anoxia is a region of hypoxia. In this region, cells are acutely short on oxygen, and their proliferation slows down or stops, but the cells themselves remain viable, and upon re-exposure to oxygen will begin to proliferate once again. Note that any sub-volumes proposed are themselves non-homogenous. As a rough estimate, a spherical tumour with a diameter of 1 cm contains 1 billion cells.[63] Furthermore, the signal from a PET scanner obviously does not have a cellular resolution. Each voxel contains millions of tumour cells. Any biological target volume developed from this method or any other intrinsically implies a statistical probability of cells belonging to one of the various populations proposed.

The process of uncovering underlying BTVs has already been started (in lung cancer patients) by Devic et al.[59] along with work on BTV volume thresholding. We wish to now explore the extension of this work from lung patients to rectal cancer patients. First, this means a thorough investigation into background definition (described in Section 2.2). In the case of lung

patients, the availabilty of a healthy contra-lateral organ led to an easier background definition, contrasted with the un-paired rectum. Furthermore, once potential BTVs are postulated within the rectal cancer patient data, we wish to move beyond thresholding to contour these volumes and to analyse them to determine if there is any significant difference between two subgroups of patients who responded differently to radiotherapy.

Chapter 2: Methods

2.1: Study Cohort

The study performed was a retrospective analysis of 15 histopathologically confirmed adenocarcinoma rectal cancer patients. For all of these patients, PET/CT scans were acquired prior to endorectal brachytherapy treatment. The patients were informed and the data was made available for this study. The PET/CT protocol was performed as the standard at the Montreal General Hospital in the past (no longer the standard). The brachytherapy (4 fractions of 6.5 Gy) was given to both potentially reduce the tumour size and lower the tumour staging. Six to eight weeks after the course of brachytherapy radiation was completed, the patients went for surgical resection of any remaining disease. Each patient was clinically staged twice: first after receiving the PET/CT scan prior to any treatment, and secondly at the time of surgical resection. The cohort was chosen such that at the time of initial staging, all patients were classified as T3N0, having disease grown into the colon or rectum and nearby tissues while having neither proximal nodal involvement nor distant metastasis. We chose all the available patients such that at the time of the second staging they fulfilled our selection criterion - an even split between T0N0 (no visible tumour) and T3N0 patients. In other words, the cohort was chosen such that given a relatively homogenous initial staging, the patients split into two populations with a large dichotomy – those which responded extremely well to radiation (complete response - T0N0), and those which responded either poorly or not at all (T3N0).

The standard hospital full-body PET/CT scan protocol was used for all patients, as detailed in Tables 1 and 2. It should be noted that while for the GE Healthcare PET scanner used, 4.687 mm is listed as the spatial resolution of the reconstructed PET image; the resolution is best

at the center of the field of view. The scanner documentation states that the full-width at half-maximum is 5 mm at the center of the image, decreasing to 6.5mm 10 cm away.[64]

Image Modality	CT Scan
KvP	140
mAs	80
Image Size (voxels)	512 x 512
Voxel Resolution	1.17 mm

Table 1: CT Scan protocol parameters

Image Modality	PET Scan
Initial ^{18}F-FDG Activity	250 MBq
Bed Positions	6
Acquisition Time	4 minutes per position
Attenuation Correction	Calculated with Rescaled CT Data
Axial Slice Width	3.27 mm
Image Size (voxels)	128 x 128
Voxel Resolution	4.687 mm

Table 2: PET Scan protocol parameters

To begin, all the PET DICOM data were collected from the hospital PACS database. The full extent of slices containing a portion of cancerous tissue was determined for each patient by observation with the use of various window and level settings for the PET images. As the project progressed, the CT DICOM data was collected as well to assist visualization (see Section 2.2). While all the voxel values extracted were taken from the PET images, CT data was able to provide tissue uniformity information when the two images were viewed together.

All work in the following subsections relating to extracting signal and background, as well as creating histograms was performed with multiple in-house MATLAB® scripts. The scripts functioned as follows: 1) Set the directory in which a patient's data is stored. 2) Read the files using "dicomread". 3) Determine maximum CT and PET value in the image series for windowing and levelling purposes. 4) Resize the PET images with "imresize" in order to match CT image size. 5) For each image slice for a patient, use "impixel" to determine a background ROI, and store the average in an array. 6) For each image, normalize by the background value for that slice uniformly. 7) Using "impoly", contour the extent of the disease, storing each voxel value in an array. 8) Using "hist" create a dUVH using all tumour voxels contoured.

2.2: Background Definition and Creating Signal to Background Ratio Images

The use of combined PET/CT imaging in determining the location of both healthy and diseased tissue requires the two images observed to be the same size. To accomplish this, a built-in MATLAB® image resize script ("imresize") was used to resample each of the 128x128 voxel PET images to simulate the 512x512 voxel CT images.

The initial PET images are acquired and saved in units of becquerels per cubic centimeter, which is a measure of radiopharmaceutical uptake. PET images are known to have multiple factors (see Section 1.3.2) that lead to machine and patient specific results, and previous work[24] has shown that signal to background images are the best option to deal with PET data quantitatively. Converting these initial raw uptake images to signal to background ratio (SBR) values offers greater insight into local physiology as it enables a direct comparison between the diseased (signal) and healthy (background) regions.

In order to create SBR images, it is required to define some specific region as the background. Typically background has been defined in PET imaging as a region of tissue that is of the same tissue type as the investigated disease, but with only healthy cells included. [24,59] We made attempts to contour regions of purely healthy rectal tissue with the guidance of the available CT scans, but this proved ultimately too difficult due to the extremely inhomogeneous structure of the site involved, and the varying presence – even slice to slice – of air pockets, fecal matter, and surrounding tissue. Figure 14 in Section 4.1 illustrates this inhomogeneity.

As a response to all these challenges, our decision was to approach background definition by setting a higher priority on tissue uniformity instead of utilizing rectal tissue *per se*. To this end, it was decided to utilize a homogeneous region of muscle tissue, away from stray signals from both the bladder and the disease, as the background. For each patient, on a slice-to-slice basis, a roughly 3 cm x 3 cm region was outlined within the muscle tissue. At first, this was performed on the PET data alone, but after obtaining the results in Section 3.1 we decided to define the ROI with the help of CT data as can be seen as a yellow square in Figure 8. From the CT image, the ROI was copied onto the PET image, and the average PET signal within the selected ROI was calculated and labelled the background uptake signal for that individual slice.

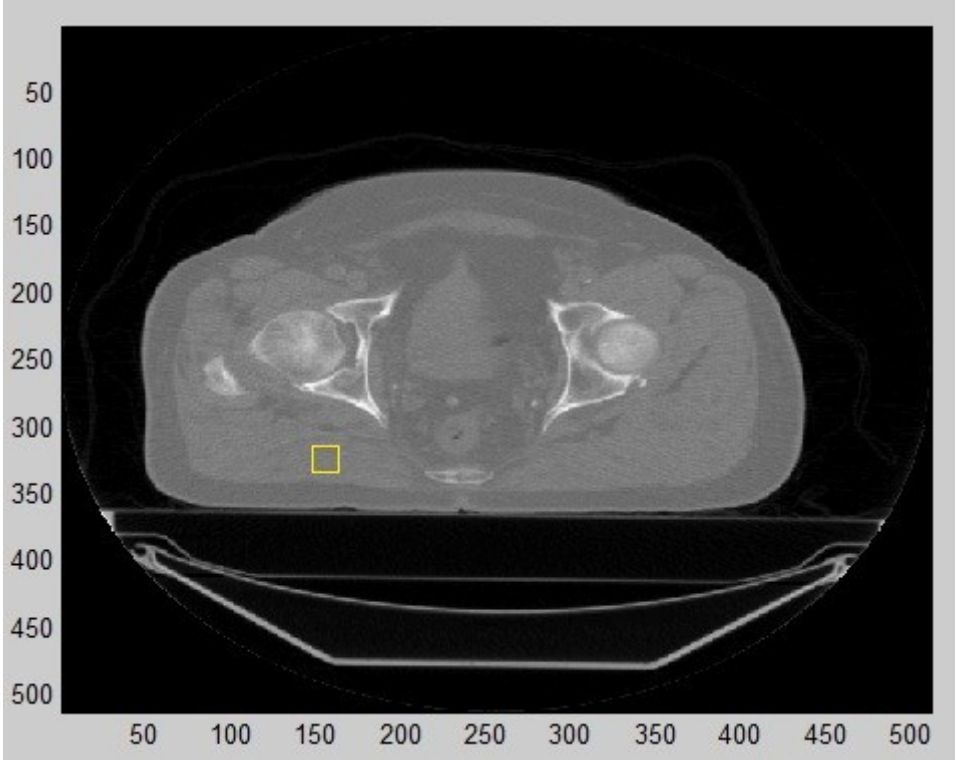

Figure 8: Definition of uniform, healthy muscle tissue in the lower left of a CT image for the determination of background signal.

Previous work[59] has created SBR images by utilizing a patient specific, uniform average background value, obtained by calculating the global mean value of every background ROI voxel in every slice for a given patient. At first, we attempted to reproduce this methodology, but this was found to be unsatisfactory, as discussed in Section 3.1. Inter-slice variation led to the decision to work with a background value for each slice. For each patient, the background ROI was sampled three times per image, and the background signal for each individual slice was calculated as the average of these three trials. Each ROI sampling for each slice, trial, and patient was drawn independently

2.3: Creation of Signal to Background Ratio Images and Region of Interest (ROI) Sampling

With background now defined for each slice, the raw PET images (in Bq/ml) were normalized to the background (also in Bq/ml) by simple division to create SBR images (unitless). To define the signal region for each PET slice, hand-drawn polygonal shapes were used to contour the diseased area. This method was used instead of an SBR threshold due to the proximity of the rectal tumours to the bladder – attempted uses of thresholding led to the accidental inclusion of undesired high-uptake voxels or the exclusion of tumour. In order to avoid any user bias, a generous margin of healthy tissue was included in each signal region to ensure all tumour voxels were sampled. An example of an ROI defined on a PET image is shown in Figure 9.

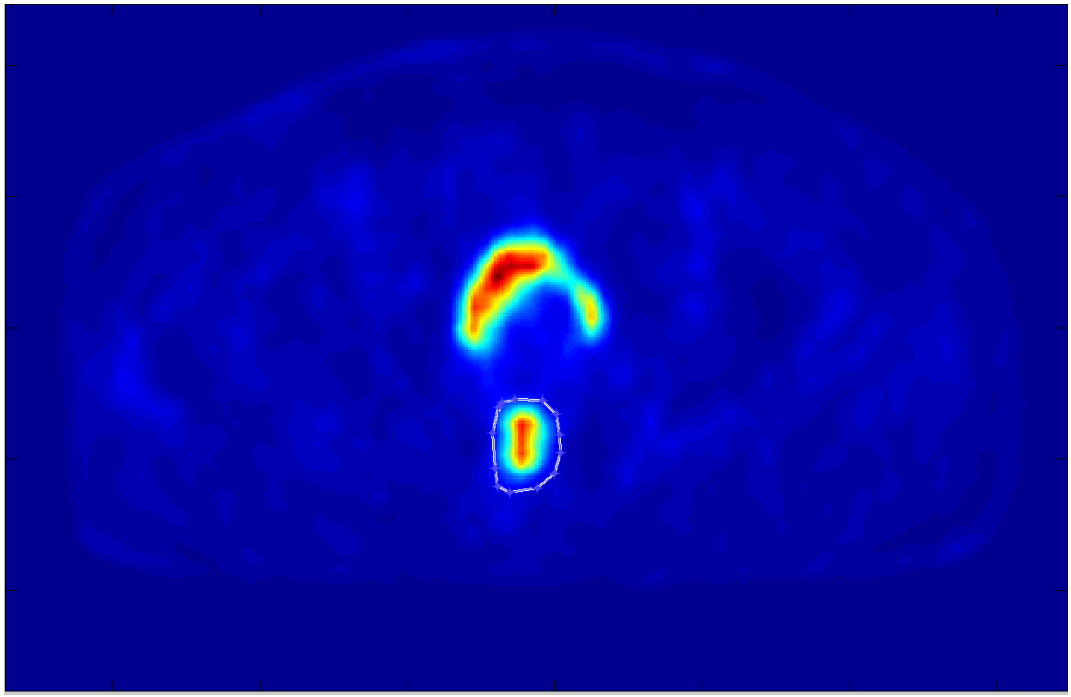

Figure 9: A manual contour surrounding a rectal tumour on one PET image. A margin of healthy tissue is given to ensure all voxels containing disease are contoured.

2.4: The Creation and Decomposition of Differential Uptake Volume Histograms

One differential uptake volume histogram (dUVH) was created for each patient. All the SBR voxel values from the multiple signal ROIs defined were collected and stored in an array. From this collection, a histogram was created corresponding to the frequency with which each SBR intensity occurred.

Each dUVH, containing a discrete number of points derived from the sampling, was converted to a probability density function (PDF) by placing the SBR uptake values in 50 bins, prior to a conversion to a continuous function. This number was chosen by adapting the number of bins (100) successfully used by Devic et al.[59] previously, taking into consideration the smaller size of the rectal adenocarcinomas investigated and thus the fewer number of voxels contained within the dUVH being decomposed. Using analytical techniques from the field of spectroscopy[65], the measured spectrum was decomposed into multiple analytical functions. The choice of number and type of analytical functions used can pose a difficult task. Traditionally in the field of spectroscopy, when presented with an unknown spectrum with uncertain origins, the best (or only) method is simply trial and error.[65] Starting with only one or two functions of the desired type, additional functions or different types of functions are added. At each stage, an optimization of the fit is performed wherein function variables such as width, area, and position are tweaked. Various methods are used to determine the level of optimization (including the χ^2 test and visual tests of logicality.) At each stage, an additional function is fit, and then optimized. In order to avoid over-fitting, the number of curves is chosen when it is observed that the addition of another curve results in either no or insignificant benefit to the level of optimization. Previous work in this field [59,66] finding that Gaussian functions worked optimally for other tumour sites led this work to be focused primarily with Gaussian functions.

A summary of the entire procedure is presented in Figure 10. This process was performed for each patient's PET/CT data. All analytical function fitting was performed with OriginPro's curve fitting package using the "Levenberg–Marquardt" quasi-Newton minimization algorithm.[67] This algorithm was not investigated as a part of the work presented here, having been validated in the field of mathematics prior to the inclusion by the software vendor. All statistical analysis was performed with Microsoft Excel's data analysis package with a p-value probability threshold of 0.05.

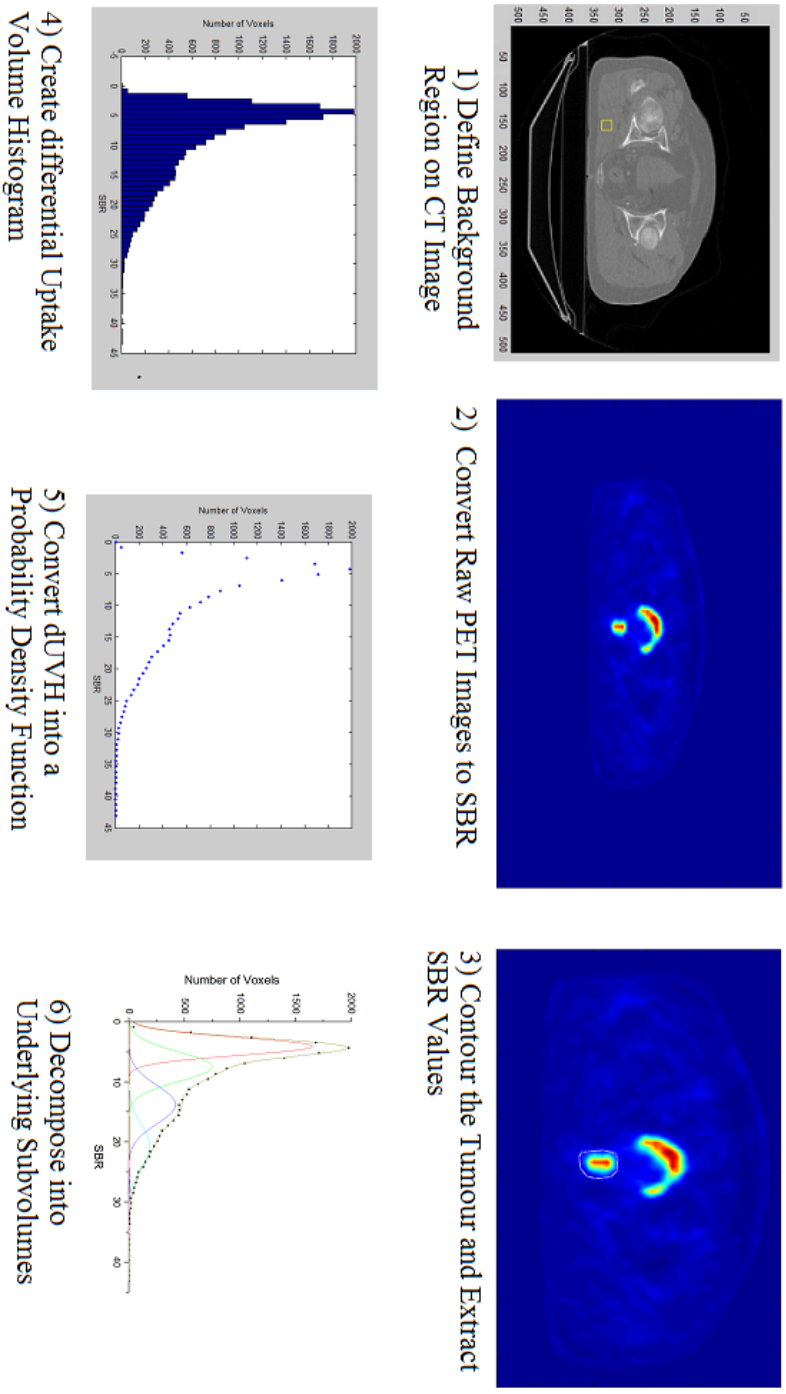

Figure 10: Summary of the dUVH Generation and Decomposition process performed for each patient.

Chapter 3: Results

3.1: Background Definition

For each patient, the background was sampled three times per slice. The average background signal was acquired in muscle for each patient. This was done at first only with the PET data. For one example patient, the three background sampling trials are shown in Figure 11 (labelled as PET Guided Trial 1/2/3), along with the mean background for each slice. After these acquisitions were performed, the methodology was changed to acquire background from the PET data after utilizing the corresponding CT image to define the background ROI. This method utilizing CT as guidance achieved the improved background signals shown for the same patient in Figure 12. For both these figures, error bars are included representing the standard deviation of background voxel signal within each background ROI contoured.

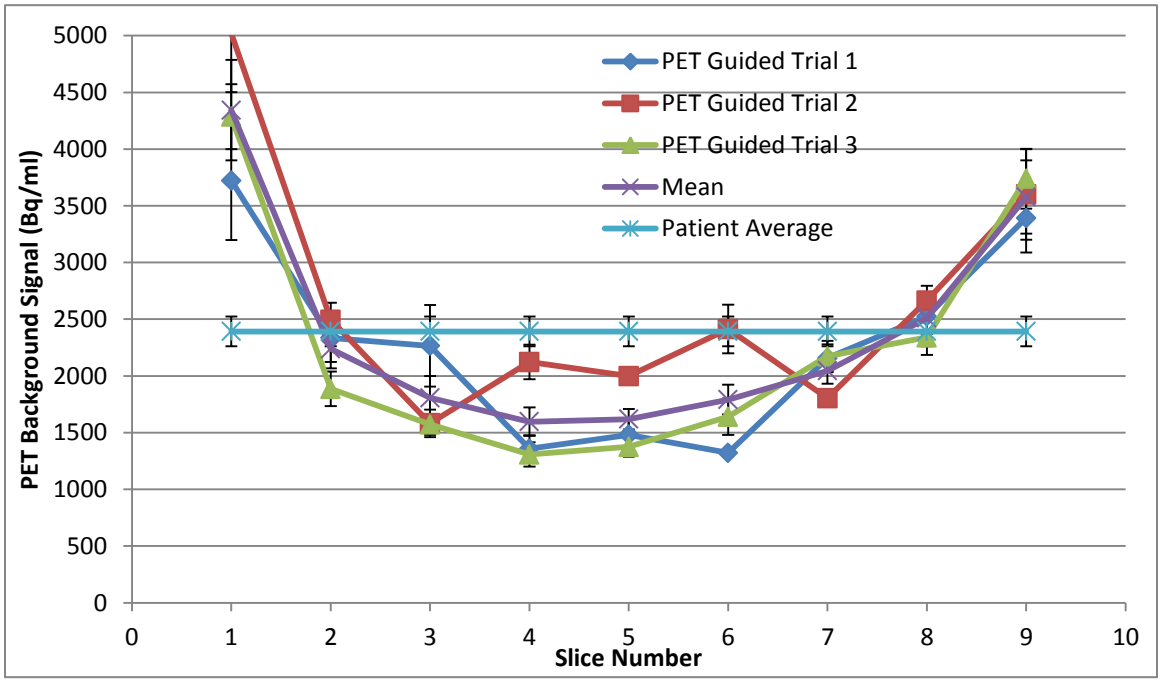

Figure 11: The background healthy muscle PET signal as determined for three trials guided with only the use of PET data, for patient #6.

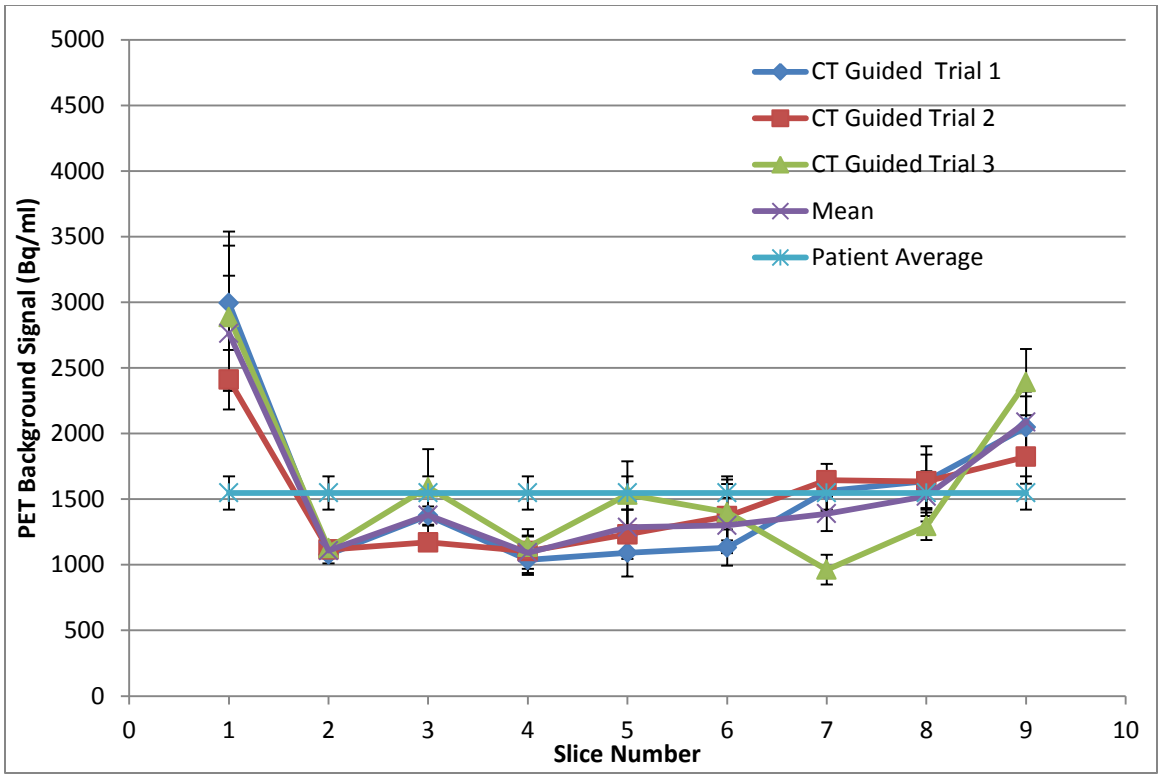

Figure 12: The background healthy muscle PET signal as determined for three trials with the use of CT images to guide sampling on the PET data, for patient #6.

In both figures, background signal was sampled three times per patient. This was done repeatedly for the same region of the same muscle in order to minimize user variability. Plotted is each trial for the given patient, as well as the mean of these trials, utilized as the background value to normalize each slice. These three background acquisition trials were then performed for each patient, with the use of CT data to visually guide background ROI selection for uniformity. Finally, the "patient average" is also plotted as a constant, reflecting the standard approach to SBR used in the past. The constant patient average mentioned and standard (and relative standard) deviation of these three trials are presented for each patient in Table 3, showing high levels of uncertainty when not taking advantage of slice-specific background definition. This led us to create SBR images utilizing a different background value for each slice.

Patient T3N0	**Mean Patient Background**	**Standard Deviation**	**Relative Standard Deviation**
1	777	76	0.10
2	998	109	0.11
3	1331	1045	0.78
4	706	361	0.51
5	1200	433	0.36
6	432	52	0.12
7	1732	589	0.34
8	391	93	0.24
T0N0			
9	452	61	0.13
10	553	94	0.17
11	317	55	0.17
12	396	45	0.11
13	923	360	0.39
14	1101	532	0.48
15	1037	528	0.51
		average:	**0.30**
		minimum:	**0.10**
		maximum:	**0.78**

Table 3: Mean patient background signal acquired (by averaging all slices together) accompanied by relative standard deviation of each slice from the patient mean.

3.2: Creation of UVHs and Subsequent Decomposition

In order to determine which analytical functions were best used to decompose the acquired PDFs, the spectroscopic trial and error method was used. Starting with prior knowledge from work done by Devic et al.[59], we used multiple Gaussian functions as opposed to other analytical functions such as Lorentzians. These Gaussian functions took the standard unnormalized form of

$$e^{\frac{-(x-\mu)^2}{2\sigma^2}}$$

The number of functions used in the decomposition was then incremented from one through to seven. Once six functions were used, the reduced χ^2 analysis results ceased to improve with a

seventh function, and as such, the patients had their PDFs decomposed with the use of six Gaussian functions. These results are presented below in Table 4. As χ^2 analysis results vary in magnitude based upon the number of voxels within a patient's dUVH, the results in this table are presented as a ratio of reduced χ^2 values, normalized to the reduced χ^2 value obtained with 6 Gaussian functions.

	Reduced Chi Square Ratio		
T3N0	**Number of Gaussians**		
Patient	**5**	**6**	**7**
1	1.25	1.00	1.31
2	3.52	1.00	2.79
3	1.01	1.00	1.38
4	7.63	1.00	5.74
5	0.98	1.00	1.40
6	1.03	1.00	1.23
7	0.98	1.00	1.66
8	1.34	1.00	1.05
T0N0			
Patient			
9	2.93	1.00	2.53
10	1.09	1.00	0.93
11	2.29	1.00	1.11
12	9.28	1.00	1.48
13	8.43	1.00	2.33
14	4.00	1.00	0.95
15	1.82	1.00	4.34

Table 4: Reduced chi-square ratios, normalized to the 6 Gaussian function result

Figure 13 shows one such Gaussian decomposition for a patient in each of the T3/T0 groups. For the rest of this thesis, these underlying Gaussian functions will be referred to as sub-volumes 1-6 (V1-V6) as labelled on Figured 13 in increasing SBR value and thus increasing FDG uptake. The term sub-volume refers to the voxels lying under each of the Gaussian

functions. These 3D sub-volumes could then be extracted by using the intersection of the Gaussian curves as a threshold.

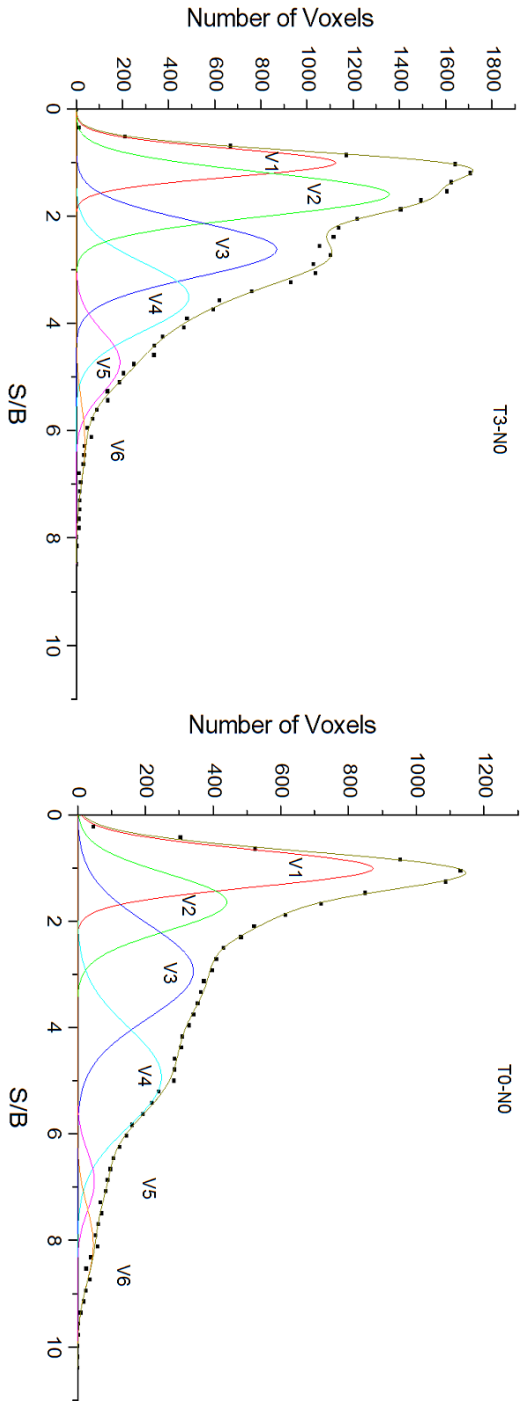

Figure 13: Volumes extracted from a decomposed PDF for each patient subgroup.

3.3: Results of Decomposition

Once the decomposition of the patients' PDFs into six analytic Gaussian functions was completed, the parameter of interest, the size of each sub-volume, in voxels, was extracted from the Gaussian fitting parameters. These values are summarized below in Table 5, along with the uncertainty as determined by the curve-fitting algorithm.

	Absolute Volume of Sub-volume (# of Voxels)					
T3N0	Sub-volume 1	2	3	4	5	6
Patient #						
1	6135 ± 61	4609 ± 82	3387 ± 89	1687 ± 91	30 ± 54	142 ± 104
2	1100 ± 18	1571 ± 24	1203 ± 25	503 ± 22	109 ± 23	155 ± 33
3	1125 ± 19	928 ± 24	353 ± 22	209 ± 21	89 ± 18	41 ± 17
4	7164 ± 102	13467 ± 135	10927 ± 165	7485 ± 187	2730 ± 155	714 ± 162
5	2543 ± 62	2480 ± 92	3156 ± 93	925 ± 70	279 ± 56	22 ± 56
6	1226 ± 17	975 ± 23	915 ± 25	106 ± 16	22 ± 12	70 ± 25
7	1058 ± 22	1706 ± 31	2321 ± 33	986 ± 28	101 ± 27	223 ± 50
8	1438 ± 59	3190 ± 86	1951 ± 95	1134 ± 91	97 ± 61	85 ± 70
T0N0						
Patient #						
9	1690 ± 32	2399 ± 43	1154 ± 47	795 ± 52	545 ± 73	182 ± 66
10	771 ±15	512 ± 20	218 ± 18	133 ± 17	24 ± 19	31 ± 24
11	7094 ± 84	5528 ± 116	7152 ± 129	5494 ± 120	641 ± 95	814 ± 107
12	7292 ± 90	7376 ± 138	8618 ± 176	4858 ± 178	3786 ± 187	1216 ± 175
13	6474 ± 102	3131 ± 61	2829 ±87	2303 ± 98	1395 ± 108	258 ± 161
14	1339 ± 37	2838 ± 56	2696 ± 73	2225 ± 90	616 ± 76	214 ± 44
15	1315 ± 25	1478 ± 35	1110 ± 39	603 ± 40	162 ± 29	13 ± 16

Table 5: Resulting volumes of each sub-volume used to decompose a PDF

As every patient's disease progression and size are unique, absolute volumes are less relevant than relative values. Instead of comparing absolute values, we introduce the concept of relative abundance. This value is defined by summing the total number of voxels, for each

patient, in the sub-volumes to be investigated, and presenting each sub-volume as a percentage of the whole tumour volume investigated. Sub-volumes 1 and 2 were excluded from the total tumour volume, for reasons discussed in detail in Section 4.1. Table 6 presents the relative abundance of each of sub-volumes 3 through 6 for each patient (such that each patient adds up to 100%), as well as the mean and standard deviation for each of the two patient subgroups. Mathematically, this can be represented as (with i = 3-6):

$$Relative\ Abundance_i = \left(\frac{Absolute\ Volume_i}{\sum_{k=3}^{6} Absolute\ Volume_k}\right) * 100$$

For sake of completeness, Table 7 further below shows each sub-volume's relative abundance calculated for each patient when including sub-volumes 1 and 2 (in other words, expanding i and k to 1-6 in the above equation). Table 8 goes on to display the worsening relative standard deviations for sub-volumes 3-6 when sub-volumes 1/2 are included and excluded.

	Sub-volume Relative Abundance (%)			
T3N0 Patient #	Sub-volume 3	4	5	6
1	64.6 ± 2.7	32.2 ± 2.0	0.6 ± 1.0	2.7 ± 2.0
2	61.1 ± 2.1	25.5 ± 1.3	5.5 ± 1.2	7.9 ± 1.7
3	51.1 ± 3.2	30.2 ± 1.9	12.9 ± 0.8	5.9 ± 0.4
4	50.0 ± 1.5	34.2 ± 1.0	12.5 ± 0.4	3.3 ± 0.1
5	72.0 ± 3.0	21.1 ± 0.9	6.4 ± 0.3	0.5 ± 0.02
6	82.3 ± 3.7	9.5 ± 0.4	2.0 ± 0.1	6.2 ± 0.3
7	63.9 ± 2.1	27.2 ± 0.9	2.8 ± 0.1	6.1 ± 0.2
8	59.7 ± 3.3	34.7 ± 1.9	3.0 ± 0.2	2.6 ± 0.1
Mean	**63.1**	**26.8**	**5.7**	**4.4**
Standard Deviation	**10.6**	**8.4**	**4.7**	**2.5**
T0N0 Patient #				
9	43.1 ± 2.6	29.7 ± 2.4	20.4 ± 2.9	6.8 ± 2.5
10	53.7 ± 6.8	32.9 ± 5.3	5.9 ± 4.7	7.5 ± 5.9
11	50.7 ± 1.2	39.0 ± 1.1	4.5 ± 0.1	5.8 ± 0.8
12	46.6 ± 1.3	26.3 ± 1.1	20.5 ± 1.1	6.6 ± 1.0
13	41.7 ± 1.9	33.9 ± 1.9	20.6 ± 1.7	3.8 ± 2.4
14	46.9 ± 1.7	38.7 ± 1.8	10.7 ± 1.3	3.7 ± 0.8
15	58.8 ± 2.9	31.9 ± 2.4	8.6 ± 1.6	0.7 ± 0.8
Mean	**48.8**	**33.2**	**13.0**	**5.0**
Standard Deviation	**6.0**	**4.6**	**7.2**	**2.4**

Table 6: Relative abundance analysis for sub-volumes 3-6

	Sub-volume Relative Abundance (%)					
T3N0 Patient #	1	2	3	4	5	6
1	38.4	28.8	21.2	10.5	0.2	0.9
2	23.7	33.9	25.9	10.8	2.3	3.3
3	41.0	33.8	12.9	7.6	3.2	1.5
4	16.9	31.7	25.7	17.6	6.4	1.7
5	27.0	26.4	33.6	9.8	3.0	0.2
6	37.0	29.4	27.6	3.2	0.7	2.1
7	16.5	26.7	36.3	15.4	1.6	3.5
8	18.2	40.4	24.7	14.4	1.2	1.1
Mean	**27.3**	**31.4**	**26.0**	**11.2**	**2.3**	**1.8**
Standard Deviation	**10.2**	**4.6**	**7.2**	**4.6**	**2.0**	**1.1**
T0N0 Patient #						
9	25.0	35.5	17.1	11.8	8.1	2.7
10	45.6	30.4	12.9	7.9	1.4	1.8
11	26.5	20.7	26.8	20.6	2.4	3.0
12	22.0	22.3	26.0	14.7	11.4	3.7
13	39.5	19.1	17.3	14.1	8.5	1.6
14	13.5	28.6	27.2	22.4	6.2	2.2
15	28.1	31.6	23.7	12.9	3.5	0.3
Mean	**28.6**	**26.9**	**21.5**	**14.9**	**5.9**	**2.2**
Standard Deviation	**10.8**	**6.2**	**5.7**	**5.0**	**3.7**	**1.1**

Table 7: Relative abundance analysis for sub-volumes 1-6

	Group	Sub-volumes Included	V3	V4	V5	V6
Relative Standard Deviation	**T3N0**	V3-6	17%	31%	82%	56%
		V1-6	28%	41%	84%	64%
	T0N0	V3-6	12%	14%	56%	48%
		V1-6	27%	34%	62%	51%

Table 8: Relative standard deviations comparing inclusion and exclusion of sub-volumes 1 and 2

3.4: Statistical Analysis

A "t-Test: Two-Sample Assuming Unequal Variances" statistical analysis was performed using Microsoft Excel's data analysis package, with the results compiled in Table 9. This was performed as we wished to investigate whether two sample means (that of each patient population which responded differently to radiotherapy) are equal or different. A p-value of 0.05 was used as the requisite for significance.

Patient Group	**Relative Abundance as % of Volumes 3-6**			
	Sub-volume 3	4	5	6
T3N0	63.1 ± 10.6	26.8 ± 8.4	5.7 ± 4.7	4.4 ± 2.5
T0N0	48.8 ± 6.0	33.2 ± 4.6	13.0 ± 7.2	5.0 ± 2.4
p-value	0.0038	0.045	0.022	0.33

Table 9: Summary of statistical comparison between the two patient groups

Chapter 4: Discussion

4.1: Methodological Evaluation

PET as an imaging modality has repeatedly been described as being disease-, patient-, and machine-specific. Hence, when a study utilizes quantitative values for comparisons between different patients, it is necessary to ensure that the values investigated are minimally susceptible to these various concerns. The concept of standardized uptake value (SUV) makes the fundamental assumption that activity would be uniformly distributed over the entire body of the patient. Without introducing the question of how, assuming perfect healthiness, the activity would distribute throughout the body given that all the body's tissues are non-uniform, the assessment of metabolic activity within a tumour should be based on normalization to some normal tissue that is held as constant as possible. This value is, of course, the signal to background ratio (SBR).[24]

For illustrative purposes, Figure 14 shows the same slice acquired by both CT (left) and PET (right) scan. As can be observed with a glance at this figure, it is very difficult to define a background in order to create SBR images in the case of rectal cancer. This difficulty arises from numerous confounding factors. First, the boundary of the rectum is itself extremely malleable. It can vary from slice to slice due to both basic shape variations as well as chronologically as imaging occurs while bodily processes are ongoing. Next, depending on the image, the region can contain pockets of air or fecal matter (as can be seen as a dark circle in the middle of the rectum on the CT image on the left of Figure 14). Finally, despite the fact that creating an outline encompassing the actual tumour is relatively easy on PET images, it is very challenging to define a ROI containing purely healthy rectal tissue, again demonstrated in Figure 14, in both images. The rectum, being located between the two very bright regions of the healthy bladder (where

waste FDG accumulates prior to removal from the body) and the actual tumour, led to increased challenges. These difficulties led to the decision to define background not as healthy rectal tissue but as healthy muscle tissue. At this point, we have not yet determined an efficient and practical way to sample healthy rectal tissue, and this approach currently represents a limitation to this methodology.

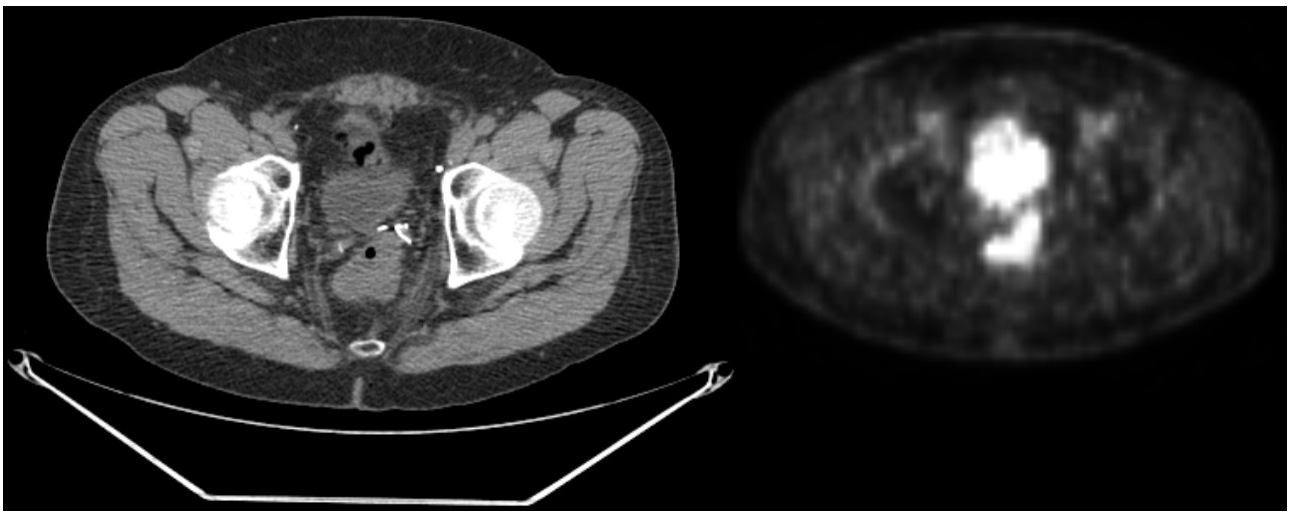

Figure 14: A single image from a joint PET/CT scan acquired for one of the patients in the study. CT scan is on the left, and PET scan is on the right.

In the initial stages of this project, it was decided to define the background signal by going through each slice containing the disease, defining a region of interest in the background portion of each slice, and create an average, patient-specific background signal intensity, as has been done in the past.[59] We decided to investigate slice to slice variation in the average background signal as well. As such, the average background signal intensity was plotted for each slice, as can be seen in one patient in Figure 11, for three different background selection trials. Traditionally, background has been defined as a single value for a patient, and all PET images were normalized to one value – which is labelled patient average in this figure. Upon seeing the

large fluctuations between not only each slice but also between each trial, it was decided that a more profound investigation was required.

The designation of background ROIs within the healthy muscle on the CT image set to be mirrored onto the PET images enabled the plotting of the average PET background signal for the same patient presented in Figure 12. As is immediately obvious, the results are less scattered. This uncertainty in ROI definition greatly led to fluctuations in background signal despite the fact that the ROI was being sampled only slightly differently each time. This can be observed by noting that the uncertainty represented by the error bars in Figures 11/12 are roughly the same, but that for each slice, the trials are clustered much closer together when using CT to visually guide ROI selection. Upon inspection (eg: Figure 14), it was determined that what appeared to be homogeneous muscle tissue on the PET scan could contain varying percentages of fat or other tissue types. As anatomical muscle tissue was easier to observe and delineate on CT images, the mirroring of CT ROIs onto PET data provided much improved results.

Despite the major improvement provided by the use of CT to define the background signal, Figure 12 shows that it is quite obvious that despite defining the background as a homogenous tissue type, there were inter-slice variations regardless. This was again reliably observed for multiple patients. When looking at Table 3, it can be seen that the relative standard deviation of each slice from a patient grand average was at absolute best 10%, reaching as high as78%, and being on average 30% for each patient. As such, the decision was made to define background for each patient not as one patient-specific average, but a set of further discretized slice-specific averages (taken over three trials).

The process of converting a patient's PET scan into a probability density function (no intrinsic formulae, beyond the summation of Gaussian functions we fit) does not intrinsically provide any additional information about the tumour itself. The creation of a PDF in some ways reduces information. In creating a PDF, any spatial information is removed. For example, knowledge of if the PDF region of highest uptake is one physically large region or multiple smaller regions of locally high uptake would not be known.[68] The net benefit of this methodology lies with the proposal that in performing signal decomposition, it becomes possible to extract information regarding underlying biological volumes of interest. In fact, when it comes to the loss of the spatial image information, efforts have been previously made to utilize the decomposition of PDFs to outline these potential biological sub-volumes using the intersections of the fit functions. [59]

In performing the decomposition itself, the literature is sparse when it comes to suggesting approaches, so the spectroscopic trial and error method was used as no fundamental information was known about the component sub-volumes. The fact that Gaussian functions have appeared to offer the best fits[59] could potentially change or evolve as future studies are conducted. An intuitive argument for Gaussians is that each potential sub-volume would have some mean uptake level, with some probability to fall on either side. Note that each of these volumes is not proposed to be uniformly of one type of cell – each voxel contains varying percentages of cells of many types. Speculatively, perhaps in other cancer sites, one lone sub-volume could have a much longer tail in one direction based on some underlying biology. Looking at Table 4, it seems clear that the choice of six Gaussian functions was the best representation of the underlying data for these rectal adenocarcinoma patients. Nearly every patient had the best curve fit with 6 functions as determined by χ^2 analysis, reduced to take into

account the degree of freedoms. While the choice of six Gaussians was found to be best in this study, it is important to note that the fundamental physiological nature of any tumour is not yet fully understood, and so the theoretical realm of future function combinations is vast.

The underlying assumption of this work is that each Gaussian used to decompose a PDF corresponds to a different and unique biological target volume within the tumour. The absolute volume contained within each of these sub-volumes in terms of voxels was recorded in Table 5. However, when reproducibility was tested, it was observed that the very first sub-volume varied dramatically from trial to trial, in terms of position, width, and height. It is suspected that this first, lowest FDG uptake, sub-volume would correspond to voxels containing non-cancerous elements – whether this would be air, fecal matter, healthy tissue, or even a partial volume averaging of one of the above and tumour is unclear. As such, it is also expected that the exact shape of this sub-volume would vary much more directly with the contouring and ROI definition than that of the others. Due to the proximity of the rectum to the bladder, it was impossible to utilize some threshold value to define the ROI as either inclusion of the bladder with too low of a threshold or exclusion of the tumour with too high of a threshold continued to occur. The necessary decision was taking to exclude sub-volume 1 from analysis – and as a corollary of this sub-volume 2. Because of the overlapping nature of the Gaussian functions fit (observe Figure 13 – for each patient, there are many voxels that correspond to either V1 or V2 as we expect from the averaging process of millions of cells in a PET voxel; thus the uncertainty in the fit on V1 results in an uncertain fit on V2). It was found that regardless of the signal ROI that was drawn, that sub-volumes 3-6 remained realistically unchanged. This is to be expected, as these sub-volumes contained predominantly cells with an above background level of uptake - which would be thus contained within the tumour and included despite any user-created fluctuations in

ROIs contoured. This follows the suggestion from the results obtained previously by Devic et al.[59] This paper found that depending on the ROI sampled (albeit in this work thresholds were utilized as lung patients were studied) the lowest-uptake regions of the dUVH were the least reproducible (see Figure 15).

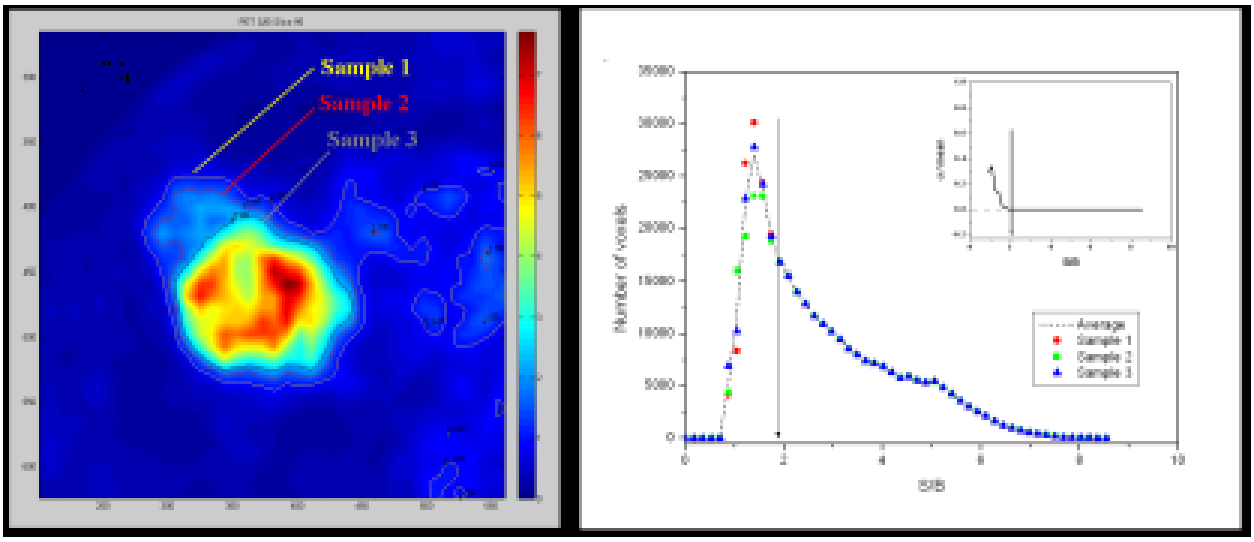

Figure 15: Three different tumour ROIs illustrating uncertainty at lower SBR values.
Image adapted from Devic et al.[59]

Due to the variability in the first sub-volume from ROI variation, the inclusion of it in the total volume denominator for relative abundance would lead to large amounts of uncertainty. This can be observed by comparing Table 6 to Table 7. When the first sub-volume was included in the relative abundance analysis, the patients had relative abundances for V1 of 27%±10% and 29%±11% for the T3N0 and T0N0 groups respectively. This large distribution of possible sub-volume 1 abundances is directly due to minor fluctuations in the manual tumour contouring. Furthermore, when comparing the means and standard deviations obtained, we see that the inclusion of sub-volumes 1 and 2 leads to uniformly worse relative standard deviation (relative meaning taking into consideration the change in total volume investigated) in Table 8.

The fact that the higher uptake sub-volumes were observed to reliably develop over the course of the decomposition enabled a direct comparison of only these sub-volumes between patients, and as such, relative abundance was defined for only sub-volumes 3 through 6. In future studies for other sites in the body, or for rectal patients with a yet further refined background definition system, it would be expected, and in fact desired, to include these potentially healthy regions. While it is only speculation, it could be theorized that detailed contouring could result in the removal of all air or fecal matter, which may, in fact, lead to the elimination of one of the included sub-volumes altogether. An ideal method for ROI definition moving forward in this field would arrive with the development of pixel-perfect registration between CT and PET images which would potentially allow the conversion of professionally outlined GTVs obtained from the clinic's radiation oncologist as outline on CT to be adapted to PET imaging.

4.2: Predictive Power of BTVs

The primary non-methodological results of this work are summarized in Table 9 above. For the cohort of patients involved in this study, a statistically significant difference in relative abundance was found between patients who achieved a complete response after undergoing brachytherapy treatments and those who did not respond at all. Of the total tumour volume investigated (sub-volumes 3 through 6), it was observed that patients with a complete response had, on average, a more glycolytic phenotype. Regarding the individual sub-volumes studied (3-6), both patient groups had the same trend of each increasingly glycolytic sub-volume comprising less of the total volume studied. The non-responders (T3N0 patients) had on average, a statistically significantly larger sub-volume 3 and smaller sub-volumes 4 and 5. The most glycolytic sub-volume, #6, was found to be statistically indistinguishable between responders

and non-responders. We postulate that this is caused in part due to the relatively small size of the sub-volume itself (being equal to roughly 5% of the tumour volume investigated), but this does not exclude a deeper biological possibility, more easily explored with larger patient cohorts or other types of studies in the future. This could be supported by the fact that glycolytic cancer cells do spend more of their time dividing (in the m phase of the cell cycle - which has been shown to be the most radiosensitive.)[19]

As described in the literature review, the prognostic capabilities in FDG-based PET imaging are continually being evaluated, and disagreements arise in the literature over the different parameters to study. To the best of our understanding, the method of decomposing dUVHs into BTVs has not been employed in prognostic studies. The closest analogy to the work performed here with relative abundances would be found in the mean SUV value of a patient's tumour. Hatt et al[55] found that the only pre-treatment variable that correlated with a positive response of rectal cancer to chemoradiotherapy was the mean SUV value of the tumour. Those that responded well were found to have $SUV_{mean} = 9.0 \pm 2.3$ and those that did not respond were found to have $SUV_{mean} = 6.4 \pm 2.9$. While this work decomposes the tumour volume into different sub-volumes, those that responded poorly having a more abundant sub-volume 3 (the least glycolytic) with 63.1% ± 10.6 of the volume studied could argue that the tumour as a whole would have a lower FDG uptake.

4.3: Future Topics of Research

When it comes to the statistical results presented in this work, it is important to note that what is being proposed here is a potential prognostic link and not a complete model. While we have shown that there was a statistically significant difference in tumour sub-volume abundance between the groups that were poorly- and well-responding to radiotherapy, the study was

designed to analyze cases of solid, single tumour patients with the greatest dichotomy in outcomes related to rectal adenocarcinoma. Besides T3N0 and T0N0 patients, studies can branch out to intermediate tumour staging such as T1N0/T2N0, implying a partial response to radiotherapy, or to determining the potential for nodal involvement (any N staging) or spread to a distant metastasis (any M staging). Once this or any other statistically relevant prognostic link is discovered and/or further verified, it would then be possible to evaluate abundance-based thresholds which could be used to categorize patients based on their initial PET scan. If proven sensitive and specific enough, this method could potentially lead to dose escalation (in the case of poor responders), reduction (in the case of complete responders), or treatment regime alteration. Furthermore, if a predominance of particular sub-volumes is proven to correlate with poor response, work is currently being done on using methodologies similar to those describe here to isolate and contour these BTVs to enable dose painting[59] – a step away from the uniform treatment typically delivered.

In addition to the complications in outlining the tumour which led to the sub-volume blurring and the exclusion of sub-volumes 1 and 2 from the study discussed in Section 4.1, there are other sources of overlap currently intrinsic to PET imaging. First, blurring is captured throughout the roughly 30 minute acquisition time. For a disease like rectal cancer, the continued activity of the digestive system can potentially cause tumour motion throughout acquisition and results in the necessity of strict adherence to fasting within a time period prior to the scan and the potential use of enemas or other clinical techniques.[69] Secondly, as mentioned in the introduction, PET images have a fairly poor spatial resolution, especially when compared with CT or MRI. Much ongoing research into both PET acquisition and reconstruction is taking place. Some current topics of interest include the partial volume effect[70], interaction depth[71], wobbling

of the scanner bed[72], and point spread function modelling for improving performance. [73] With every improvement to PET scan quality and voxel resolution, the type of work presented in this thesis will only improve in accuracy and precision.

The entirety of the work presented in this document is for the use of FDG. FDG is by far the most common radiopharmaceutical in use today – it is relatively cheap to produce or acquire, and the protocols for its use are well spread and understood. This and other studies of FDG for the purpose of uncovering and evaluating BTVs focus purely on the glycolytic uptake of the tumour. There are a large number of others being produced for academic or clinical purposes, and the use of these other radiopharmaceuticals can offer either complementary information regarding BTVs or potentially radically novel information. One more recently prominent compound is ^{18}F–FMISO. Originally a chemotherapy agent based on nitroimidazole conjugates of bis(thiosemicarbazonato)^{64}Cu(II), ^{18}F–FMISO has been shown to act as a marker of hypoxia.[74] The presence and size of hypoxic volumes obtained could give complementary information, and in fact, assist in determining whether or not a sub-volume found from the decomposition of FDG dUVHs corresponded to a hypoxic volume.

It would be of immense value to the study of biological target volumes to commission a longitudinal study of patients undergoing radiotherapy. Along with the previous work mentioned in the introduction, others have found that the evolution of FDG PET signals has been a successful predictive factor in determining the histopathological response of rectal tumours after radiochemotherapy.[75] The ability to decompose differential uptake volume histograms for the same patient over the course of treatment would test the hypothesis of whether these BTVs are distinct and consistent structures – and furthermore to test if certain patterns of sub-volume evolution over time could be harnessed for prognostic capability.

Chapter 5: Summary and Conclusions

The introduction of FDG-based PET imaging has revolutionized the world of functional imaging. As a complementary modality to anatomy based CT or MR imaging, PET allows the investigation of the underlying biological nature of a tumour. Much focus in current research is directed towards the use of PET data to re-define the clinical CT-based GTV, which is considered the gold standard. Based on the formative paper by Ling et al[20], we believe that these multidimensional modalities should be used in a complimentary fashion, instead of trying to replace one with the other. Our goal is to use PET data to define and outline multiple biological target volumes within a tumour, as well as evaluate the potential prognostic capabilities of these BTVs, once defined.

In this work, we detail a methodology for the unveiling of potential biological sub-volumes from FDG-based PET data. The method starts with the creation of signal to background ratio (SBR) images from the raw FDG PET uptake images acquired. In turn, we used these SBR images to create differential uptake volume histograms (dUVHs) from regions of interest containing the extent of the disease, which are then used to create probability density functions (PDFs). Following the spectroscopic method, signal decomposition was performed on these PDFs, to uncover these potential biological sub-volumes based on glycolytic activity.

We tested this methodology on pre-therapy images of 15 patients treated in our department for rectal adenocarcinoma. The cohort was chosen such that at the time of PET/CT imaging, all patients were staged as T3N0. After imaging, they all went for brachytherapy treatments before surgery. At the time of surgery, eight of the patients had not responded to the radiotherapy, and seven had a complete response. We wished to look into the differences in uncovered sub-volumes between these two sub-groups.

For each patient, we first converted the raw PET images to SBR images. In the study of SBR images, the fundamental definition of background signal is essential. In the case of a tumour site such as the rectum, the definition of healthy rectal tissue alone is difficult due to the malleable nature of the rectum, as well as the fact that it can contain both air and fecal matter pockets. To improve consistency, we used a background signal definition process in which the signal is determined on a slice-by-slice basis (as contrasted with a uniform patient-average), within a region of homogeneous muscle tissue sampled three times for reliability. This process was guided by CT imaging to ensure tissue homogeneity, while the actual sampling was performed on PET images.

Once SBR images were created, regions of interest containing the extent of the tumour were outlined. The SBR values contained within the ROIs were then binned to create a dUVH. After converting the dUVH to a continuous PDF, the trial and error spectroscopic method of signal decomposition resulted in the continued evolution of the PDF into six Gaussian functions (as determined by χ^2 analysis).

We argue that some of these six analytical functions that routinely developed in the process of signal decomposition may represent potential biological target volumes. These sub-volumes could potentially be linked to healthy tissue, regions of necrosis or apoptosis, and tumour cells of varying levels of glycolysis. In performing the signal decomposition, it was observed that the lowest uptake sub-volume routinely varied immensely with repeated signal ROI definition. This was concluded to correspond to either normal tissue or air/fecal matter as any glycolytic cell would be sampled in the ROIs drawn and because the higher uptake sub-volumes routinely evolved identically throughout the decomposition process.

The values of interest in our prognostic study were that of the sub-volume size. As every patient has a different gross tumour size, the absolute volume was not a relevant value to investigate. Therefore, we introduced the concept of relative abundance. This is simply the percentage of the tumour volume studied that a component sub-volume occupied. In the case of our study, we defined relative abundance as a percentage of the sum over sub-volumes 3-6 due to the variability in sub-volume 1 (and thus also 2 due to Gaussian function overlap as discussed in Section 4.1).

When comparing the relative abundances between the T3N0 and T0N0 patients, we observed with statistical significance that patients with a complete response had, on average, a more pronounced glycolytic phenotype. While between both populations the smallest sub-volume 6 (most glycolytic) was not found to be significantly different, sub-volumes 4 and 5 were more abundant in the responding subgroup, and sub-volume 3 (least glycolytic) was most abundant in the poor responders. Despite the ambiguities in the literature presented in Section 1.3.3, our findings that more aggressive tumour phenotypes were observed to be more radiosensitive are unsurprising, It is known in the field of radiobiology[19] that more aggressive cancer cells spend more of their time dividing, which means that they spend more of their time in the m phase of the cell cycle which has been shown to be the most radiosensitive.[19]

This look into the first prognostic use of dUVH decomposition and its resulting sub-volumes proves promising and leaves open numerous ways to expand and utilize the techniques described. If continued work in this field verifies that the relative abundance of certain sub-volumes has predictive qualities, then this would open up the field of potential treatment alteration for patients at the time of PET scan. If a patient's tumour could be classified as likely

to respond well or poorly with sufficient specificity and selectivity, this could result in dose reduction or escalation respectively.

Looking to the future, studies consisting of multiple scans over time would enable the observation of these BTVs and investigation into their chronological persistence. While all work presented here was based on the use of the widely available FDG radiopharmaceutical, work with other radiopharmaceuticals such as the hypoxia tracer F^{18}-MISO could lead to the definition and confirmation of hypoxic BTVs.

Altogether, the work presented here elaborates and demonstrates some of the fundamental methodological steps required to define biological target volumes. We have shown statistically significant differences in these potential BTVs for two subgroups of patient with drastically different responses to radiotherapy. Continued efforts and expanded studies within this field have the potential to advance the integration of PET data into the clinic and into the planning and evaluation of radiotherapy treatment itself on a patient to patient basis.

Chapter 6: References

1. L'Annunziata, M. F., *Radioactivity: Introduction and History*. Elsevier Science: 2007.
2. Cherry, S. R.; Sorenson, J. A.; Phelps, M. E., *Physics in Nuclear Medicine*. Elsevier Health Sciences: 2012.
3. Buck, A. K.; Herrmann, K.; Stargardt, T.; Dechow, T.; Krause, B. J.; Schreyogg, J., Economic evaluation of PET and PET/CT in oncology: evidence and methodologic approaches. *Journal of nuclear medicine technology* **2010,** *38* (1), 6-17.
4. Podgoršak, E. B.; Agency, I. A. E., *Radiation Oncology Physics: A Handbook for Teachers and Students*. International Atomic Energy Agency: 2005.
5. St James, S.; Thompson, C. J., Image blurring due to light-sharing in PET block detectors. *Med Phys* **2006,** *33* (2), 405-10.
6. Tomic, N.; Thompson, C. J.; Casey, M. E., Investigation of the "Block Effect" on spatial resolution in PET detectors. *IEEE Transactions on Nuclear Science* **2005,** *52* (3), 599-605.
7. Saha, G. B., *Basics of PET Imaging: Physics, Chemistry, and Regulations*. Springer International Publishing: 2015.
8. Sadava, D. E.; Hillis, D. M.; Heller, H. C.; Berenbaum, M., *Life: The Science of Biology*. W. H. Freeman: 2009.
9. Devic, S., Warburg Effect - a Consequence or the Cause of Carcinogenesis? *Journal of Cancer* **2016,** *7* (7), 817-822.
10. Pauwels, E.; Ribeiro, M.; Stoot, J.; McCready, V.; Bourguignon, M.; Maziere, B., FDG accumulation and tumor biology. *Nuclear medicine and biology* **1998,** *25* (4), 317-322.
11. Krebs, H. A., The Pasteur effect and the relations between respiration and fermentation. *Essays in biochemistry* **1971,** *8*, 1-34.
12. Warburg, O. H.; Dickens, F.; biologie, K. W. I. f., *The Metabolism of Tumours: Investigations from the Kaiser Wilhelm Institute for Biology, Berlin-Dahlem*. Richard R. Smith: 1931.
13. Kroemer, G., Mitochondria in cancer. *Oncogene* **0000,** *25* (34), 4630-4632.
14. Gatenby, R. A.; Gillies, R. J., Why do cancers have high aerobic glycolysis? *Nature reviews. Cancer* **2004,** *4* (11), 891-9.

15. Higashi, K.; Ueda, Y.; Sakurai, A.; Wang, X. M.; Xu, L.; Murakami, M.; Seki, H.; Oguchi, M.; Taki, S.; Nambu, Y.; Tonami, H.; Katsuda, S.; Yamamoto, I., Correlation of Glut-1 glucose transporter expression with. *European journal of nuclear medicine* **2000,** *27* (12), 1778-85.

16. Jones, D., ICRU Report 50—Prescribing, Recording and Reporting Photon Beam Therapy. *Medical Physics* **1994,** *21* (6), 833-834.

17. Beyer, T.; Townsend, D. W.; Brun, T.; Kinahan, P. E.; Charron, M.; Roddy, R.; Jerin, J.; Young, J.; Byars, L.; Nutt, R., A combined PET/CT scanner for clinical oncology. *Journal of nuclear medicine : official publication, Society of Nuclear Medicine* **2000,** *41* (8), 1369-79.

18. Zaidi, H., *Quantitative Analysis in Nuclear Medicine Imaging*. Springer US: 2006.

19. Hall, E. J.; Giaccia, A. J., *Radiobiology for the Radiologist*. Lippincott Williams & Wilkins: 2006.

20. Ling, C. C.; Humm, J.; Larson, S.; Amols, H.; Fuks, Z.; Leibel, S.; Koutcher, J. A., Towards multidimensional radiotherapy (MD-CRT): biological imaging and biological conformality. *International Journal of Radiation Oncology • Biology • Physics* **2000,** *47* (3), 551-560.

21. Nestle, U.; Walter, K.; Schmidt, S.; Licht, N.; Nieder, C.; Motaref, B.; Hellwig, D.; Niewald, M.; Ukena, D.; Kirsch, C. M.; Sybrecht, G. W.; Schnabel, K., ¹⁸F-Deoxyglucose positron emission tomography (FDG-PET) for the planning of radiotherapy in lung cancer: high impact in patients with atelectasis 2. *International Journal of Radiation Oncology • Biology • Physics* **1999,** *44* (3), 593-597.

22. Paulino, A. C.; Johnstone, P. A., FDG-PET in radiotherapy treatment planning: Pandora's box? *International journal of radiation oncology, biology, physics* **2004,** *59* (1), 4-5.

23. Black, Q. C.; Grills, I. S.; Kestin, L. L.; Wong, C.-Y. O.; Wong, J. W.; Martinez, A. A.; Yan, D., Defining a radiotherapy target with positron emission tomography. *International Journal of Radiation Oncology • Biology • Physics* **2004,** *60* (4), 1272-1282.

24. Erdi, Y. E.; Mawlawi, O.; Larson, S. M.; Imbriaco, M.; Yeung, H.; Finn, R.; Humm, J. L., Segmentation of lung lesion volume by adaptive positron emission tomography image thresholding. *Cancer* **1997,** *80* (12 Suppl), 2505-9.

25. Mah, K.; Caldwell, C. B.; Ung, Y. C.; Danjoux, C. E.; Balogh, J. M.; Ganguli, S. N.; Ehrlich, L. E.; Tirona, R., The impact of (18)FDG-PET on target and critical organs in CT-based

treatment planning of patients with poorly defined non-small-cell lung carcinoma: a prospective study. *International journal of radiation oncology, biology, physics* **2002,** *52* (2), 339-50.

26. Mutic, S.; Grigsby, P. W.; Low, D. A.; Dempsey, J. F.; Harms, W. B.; Laforest, R.; Bosch, W. R.; Miller, T. R., PET-guided three-dimensional treatment planning of intracavitary gynecologic implants. *International journal of radiation oncology, biology, physics* **2002,** *52* (4), 1104-10.

27. Vanuytsel, L. J.; Vansteenkiste, J. F.; Stroobants, S. G.; De Leyn, P. R.; De Wever, W.; Verbeken, E. K.; Gatti, G. G.; Huyskens, D. P.; Kutcher, G. J., The impact of (18)F-fluoro-2-deoxy-D-glucose positron emission tomography (FDG-PET) lymph node staging on the radiation treatment volumes in patients with non-small cell lung cancer. *Radiotherapy and oncology : journal of the European Society for Therapeutic Radiology and Oncology* **2000,** *55* (3), 317-24.

28. Ciernik, I. F.; Dizendorf, E.; Baumert, B. G.; Reiner, B.; Burger, C.; Davis, J. B.; Lutolf, U. M.; Steinert, H. C.; Von Schulthess, G. K., Radiation treatment planning with an integrated positron emission and computer tomography (PET/CT): a feasibility study. *International journal of radiation oncology, biology, physics* **2003,** *57* (3), 853-63.

29. Grills, I. S.; Yan, D.; Martinez, A. A.; Vicini, F. A.; Wong, J. W.; Kestin, L. L., Potential for reduced toxicity and dose escalation in the treatment of inoperable non-small-cell lung cancer: a comparison of intensity-modulated radiation therapy (IMRT), 3D conformal radiation, and elective nodal irradiation. *International journal of radiation oncology, biology, physics* **2003,** *57* (3), 875-90.

30. Lee, Y. K.; Cook, G.; Flower, M. A.; Rowbottom, C.; Shahidi, M.; Sharma, B.; Webb, S., Addition of 18F-FDG-PET scans to radiotherapy planning of thoracic lymphoma. *Radiotherapy and oncology : journal of the European Society for Therapeutic Radiology and Oncology* **2004,** *73* (3), 277-83.

31. van Der Wel, A.; Nijsten, S.; Hochstenbag, M.; Lamers, R.; Boersma, L.; Wanders, R.; Lutgens, L.; Zimny, M.; Bentzen, S. M.; Wouters, B.; Lambin, P.; De Ruysscher, D., Increased therapeutic ratio by 18FDG-PET CT planning in patients with clinical CT stage N2-N3M0 non-small-cell lung cancer: a modeling study. *International journal of radiation oncology, biology, physics* **2005,** *61* (3), 649-55.

32. Erdi, Y. E.; Rosenzweig, K.; Erdi, A. K.; Macapinlac, H. A.; Hu, Y. C.; Braban, L. E.; Humm, J. L.; Squire, O. D.; Chui, C. S.; Larson, S. M.; Yorke, E. D., Radiotherapy treatment

planning for patients with non-small cell lung cancer using positron emission tomography (PET). *Radiotherapy and oncology : journal of the European Society for Therapeutic Radiology and Oncology* **2002,** *62* (1), 51-60.

33. Miller, T. R.; Grigsby, P. W., Measurement of tumor volume by PET to evaluate prognosis in patients with advanced cervical cancer treated by radiation therapy. *International journal of radiation oncology, biology, physics* **2002,** *53* (2), 353-9.

34. Bradley, J.; Thorstad, W. L.; Mutic, S.; Miller, T. R.; Dehdashti, F.; Siegel, B. A.; Bosch, W.; Bertrand, R. J., Impact of FDG-PET on radiation therapy volume delineation in non-small-cell lung cancer. *International journal of radiation oncology, biology, physics* **2004,** *59* (1), 78-86.

35. Wahab, S. H.; Malyapa, R. S.; Mutic, S.; Grigsby, P. W.; Deasy, J. O.; Miller, T. R.; Zoberi, I.; Low, D. A., A treatment planning study comparing HDR and AGIMRT for cervical cancer. *Med Phys* **2004,** *31* (4), 734-43.

36. Ciernik, I. F.; Huser, M.; Burger, C.; Davis, J. B.; Szekely, G., Automated functional image-guided radiation treatment planning for rectal cancer. *International journal of radiation oncology, biology, physics* **2005,** *62* (3), 893-900.

37. Drever, L.; Robinson, D. M.; McEwan, A.; Roa, W., A local contrast based approach to threshold segmentation for PET target volume delineation. *Med Phys* **2006,** *33* (6), 1583-94.

38. Ford, E. C.; Kinahan, P. E.; Hanlon, L.; Alessio, A.; Rajendran, J.; Schwartz, D. L.; Phillips, M., Tumor delineation using PET in head and neck cancers: threshold contouring and lesion volumes. *Med Phys* **2006,** *33* (11), 4280-8.

39. Biehl, K. J.; Kong, F. M.; Dehdashti, F.; Jin, J. Y.; Mutic, S.; El Naqa, I.; Siegel, B. A.; Bradley, J. D., 18F-FDG PET definition of gross tumor volume for radiotherapy of non-small cell lung cancer: is a single standardized uptake value threshold approach appropriate? *Journal of nuclear medicine : official publication, Society of Nuclear Medicine* **2006,** *47* (11), 1808-12.

40. Brambilla, M.; Matheoud, R.; Secco, C.; Loi, G.; Krengli, M.; Inglese, E., Threshold segmentation for PET target volume delineation in radiation treatment planning: the role of target-to-background ratio and target size. *Med Phys* **2008,** *35* (4), 1207-13.

41. El-Bassiouni, M.; Ciernik, I. F.; Davis, J. B.; El-Attar, I.; Reiner, B.; Burger, C.; Goerres, G. W.; Studer, G. M., [18FDG] PET-CT-based intensity-modulated radiotherapy treatment

planning of head and neck cancer. *International journal of radiation oncology, biology, physics* **2007,** *69* (1), 286-93.

42. Schaefer, A.; Kremp, S.; Hellwig, D.; Rube, C.; Kirsch, C. M.; Nestle, U., A contrast-oriented algorithm for FDG-PET-based delineation of tumour volumes for the radiotherapy of lung cancer: derivation from phantom measurements and validation in patient data. *European journal of nuclear medicine and molecular imaging* **2008,** *35* (11), 1989-99.

43. Aristophanous, M.; Penney, B. C.; Martel, M. K.; Pelizzari, C. A., A Gaussian mixture model for definition of lung tumor volumes in positron emission tomography. *Med Phys* **2007,** *34* (11), 4223-35.

44. Li, H.; Thorstad, W. L.; Biehl, K. J.; Laforest, R.; Su, Y.; Shoghi, K. I.; Donnelly, E. D.; Low, D. A.; Lu, W., A novel PET tumor delineation method based on adaptive region-growing and dual-front active contours. *Med Phys* **2008,** *35* (8), 3711-21.

45. Prieto, E.; Lecumberri, P.; Pagola, M.; Gomez, M.; Bilbao, I.; Ecay, M.; Penuelas, I.; Marti-Climent, J. M., Twelve automated thresholding methods for segmentation of PET images: a phantom study. *Phys Med Biol* **2012,** *57* (12), 3963-80.

46. Zaidi, H.; El Naqa, I., PET-guided delineation of radiation therapy treatment volumes: a survey of image segmentation techniques. *European journal of nuclear medicine and molecular imaging* **2010,** *37* (11), 2165-87.

47. van Dalen, J. A.; Hoffmann, A. L.; Dicken, V.; Vogel, W. V.; Wiering, B.; Ruers, T. J.; Karssemeijer, N.; Oyen, W. J., A novel iterative method for lesion delineation and volumetric quantification with FDG PET. *Nuclear medicine communications* **2007,** *28* (6), 485-93.

48. Drever, L.; Roa, W.; McEwan, A.; Robinson, D., Iterative threshold segmentation for PET target volume delineation. *Med Phys* **2007,** *34* (4), 1253-65.

49. Nestle, U.; Kremp, S.; Schaefer-Schuler, A.; Sebastian-Welsch, C.; Hellwig, D.; Rube, C.; Kirsch, C. M., Comparison of different methods for delineation of 18F-FDG PET-positive tissue for target volume definition in radiotherapy of patients with non-Small cell lung cancer. *Journal of nuclear medicine : official publication, Society of Nuclear Medicine* **2005,** *46* (8), 1342-8.

50. Devic, S.; Tomic, N.; Faria, S.; Menard, S.; Lisbona, R.; Lehnert, S., Defining radiotherapy target volumes using 18F-fluoro-deoxy-glucose positron emission

tomography/computed tomography: still a Pandora's box? *International journal of radiation oncology, biology, physics* **2010,** *78* (5), 1555-62.

51. Schinagl, D. A.; Vogel, W. V.; Hoffmann, A. L.; van Dalen, J. A.; Oyen, W. J.; Kaanders, J. H., Comparison of five segmentation tools for 18F-fluoro-deoxy-glucose-positron emission tomography-based target volume definition in head and neck cancer. *International journal of radiation oncology, biology, physics* **2007,** *69* (4), 1282-9.

52. Greco, C.; Nehmeh, S. A.; Schoder, H.; Gonen, M.; Raphael, B.; Stambuk, H. E.; Humm, J. L.; Larson, S. M.; Lee, N. Y., Evaluation of different methods of 18F-FDG-PET target volume delineation in the radiotherapy of head and neck cancer. *American journal of clinical oncology* **2008,** *31* (5), 439-45.

53. Guillem, J. G.; Moore, H. G.; Akhurst, T.; Klimstra, D. S.; Ruo, L.; Mazumdar, M.; Minsky, B. D.; Saltz, L.; Wong, W. D.; Larson, S., Sequential preoperative fluorodeoxyglucose-positron emission tomography assessment of response to preoperative chemoradiation: a means for determining longterm outcomes of rectal cancer. *Journal of the American College of Surgeons* **2004,** *199* (1), 1-7.

54. Ruby, J. A.; Leibold, T.; Akhurst, T. J.; Shia, J.; Saltz, L. B.; Mazumdar, M.; Riedel, E. R.; Larson, S. M.; Guillem, J. G., FDG-PET assessment of rectal cancer response to neoadjuvant chemoradiotherapy is not associated with long-term prognosis: a prospective evaluation. *Diseases of the colon and rectum* **2012,** *55* (4), 378-86.

55. Hatt, M.; van Stiphout, R.; le Pogam, A.; Lammering, G.; Visvikis, D.; Lambin, P., Early prediction of pathological response in locally advanced rectal cancer based on sequential 18F-FDG PET. *Acta oncologica (Stockholm, Sweden)* **2013,** *52* (3), 619-26.

56. Park, J.; Chang, K. J.; Seo, Y. S.; Byun, B. H.; Choi, J. H.; Moon, H.; Lim, I.; Kim, B. I.; Choi, C. W.; Lim, S. M., Tumor SUVmax Normalized to Liver Uptake on (18)F-FDG PET/CT Predicts the Pathologic Complete Response After Neoadjuvant Chemoradiotherapy in Locally Advanced Rectal Cancer. *Nuclear medicine and molecular imaging* **2014,** *48* (4), 295-302.

57. Nestle, U.; Kremp, S.; Grosu, A. L., Practical integration of [18F]-FDG-PET and PET-CT in the planning of radiotherapy for non-small cell lung cancer (NSCLC): the technical basis, ICRU-target volumes, problems, perspectives. *Radiotherapy and oncology : journal of the European Society for Therapeutic Radiology and Oncology* **2006,** *81* (2), 209-25.

58. Mac Manus, M.; Hicks, R. J.; Everitt, S., Role of PET-CT in the optimization of thoracic radiotherapy. *Journal of thoracic oncology : official publication of the International Association for the Study of Lung Cancer* **2006,** *1* (1), 81-4.

59. Devic, S.; Mohammed, H.; Tomic, N.; Aldelaijan, S.; De Blois, F.; Seuntjens, J.; Lehnert, S.; Faria, S., FDG-PET-based differential uptake volume histograms: a possible approach towards definition of biological target volumes. *Br J Radiol* **2016,** *89* (1062), 20150388.

60. Thomlinson, R. H.; Gray, L. H., The Histological Structure of Some Human Lung Cancers and the Possible Implications for Radiotherapy. *British Journal of Cancer* **1955,** *9* (4), 539-549.

61. Nias, A. H. W., *An Introduction to Radiobiology*. Wiley: 1998.

62. Joiner, M. C.; van der Kogel, A., *Basic Clinical Radiobiology, Fifth Edition*. Taylor & Francis: 2016.

63. Friberg, S.; Mattson, S., On the growth rates of human malignant tumors: implications for medical decision making. *Journal of surgical oncology* **1997,** *65* (4), 284-97.

64. GE Healthcare, Common Documentation Library. http://apps.gehealthcare.com/servlet/ClientServlet?REQ=RNEW&MODALITY=PET (accessed 8/8/16).

65. Thorne, A., *Spectrophysics*. Springer Netherlands: 2012.

66. Mohammed, H. Differential uptake volume histograms: a novel avenue for integration of PET data into radiotherapy treatment planning. McGill University, 2011.

67. OriginLab. 15.5.3 Theory of Nonlinear Curve Fitting. http://www.originlab.com/doc/Origin-Help/NLFit-Theory (accessed July 16th).

68. Drzymala, R. E.; Mohan, R.; Brewster, L.; Chu, J.; Goitein, M.; Harms, W.; Urie, M., Three-Dimensional Photon Treatment Planning Report of the Collaborative Working Group on the Evaluation of Treatment Planning for External Photon Beam RadiotherapyDose-volume histograms. *International Journal of Radiation Oncology*Biology*Physics* **1991,** *21* (1), 71-78.

69. Miraldi, F.; Vesselle H Fau - Faulhaber, P. F.; Faulhaber Pf Fau - Adler, L. P.; Adler Lp Fau - Leisure, G. P.; Leisure, G. P., Elimination of artifactual accumulation of FDG in PET imaging of colorectal cancer. (0363-9762 (Print)).

70. Kirov, A. S.; Piao, J. Z.; Schmidtlein, C. R., Partial volume effect correction in PET using regularized iterative deconvolution with variance control based on local topology. *Phys Med Biol* **2008,** *53* (10), 2577-91.

71. Yang, Y.; Wu, Y.; Qi, J.; St James, S.; Du, H.; Dokhale, P. A.; Shah, K. S.; Farrell, R.; Cherry, S. R., A prototype PET scanner with DOI-encoding detectors. *Journal of nuclear medicine : official publication, Society of Nuclear Medicine* **2008,** *49* (7), 1132-40.

72. Suk, J. Y.; Thompson, C. J.; Labuda, A.; Goertzen, A. L., Improvement of the spatial resolution of the MicroPET R4 scanner by wobbling the bed. *Med Phys* **2008,** *35* (4), 1223-31.

73. Lee, Y. S.; Kim, J. S.; Kim, K. M.; Kang, J. H.; Lim, S. M.; Kim, H. J., Performance measurement of PSF modeling reconstruction (True X) on Siemens Biograph TruePoint TrueV PET/CT. *Annals of nuclear medicine* **2014,** *28* (4), 340-8.

74. Peeters, S. G. J. A.; Zegers, C. M. L.; Lieuwes, N. G.; van Elmpt, W.; Eriksson, J.; van Dongen, G. A. M. S.; Dubois, L.; Lambin, P., A Comparative Study of the Hypoxia PET Tracers [18F]HX4, [18F]FAZA, and [18F]FMISO in a Preclinical Tumor Model. *International Journal of Radiation Oncology*Biology*Physics* **2015,** *91* (2), 351-359.

75. Goldberg, N.; Kundel, Y.; Purim, O.; Bernstine, H.; Gordon, N.; Morgenstern, S.; Idelevich, E.; Wasserberg, N.; Sulkes, A.; Groshar, D.; Brenner, B., Early prediction of histopathological response of rectal tumors after one week of preoperative radiochemotherapy using 18 F-FDG PET-CT imaging. A prospective clinical study. *Radiation oncology (London, England)* **2012,** *7*, 124.